Linking sediment supply variations and tectonic evolution in deep time, source-to-sink systems—The Triassic Greater Barents Sea Basin

Albina Gilmullina[1,†], Tore Grane Klausen[2,§], Anthony George Doré[3,§], Valentina Marzia Rossi[4,§], Anna Suslova[5,§], and Christian Haug Eide[1,§]

[1]*Department of Earth Science, University of Bergen, Allégaten 41, 5007 Bergen, Norway*
[2]*MVest Energy AS, Edvard Griegs vei 3, 5059 Bergen, Norway*
[3]*Energy & Geoscience Institute (EGI), University of Utah, 423 Wakara Way, Suite 300, Salt Lake City, Utah 84108, USA*
[4]*Italian National Research Council, Institute of Geosciences and Georesources, Via Adolfo Ferrata, 1, I-27100 Pavia, Italy*
[5]*Petroleum Department, Lomonosov Moscow State University, 1 Leninskiye Gory, 119991 Moscow, Russia*

ABSTRACT

Triassic strata in the Greater Barents Sea Basin are important records of geodynamic activity in the surrounding catchments and sediment transport in the Arctic basins. This study is the first attempt to investigate the evolution of these source areas through time. Our analysis of sediment budgets from subsurface data in the Greater Barents Sea Basin and application of the BQART approach to estimate catchment properties shows that (1) during the Lower Triassic, sediment supply was at its peak in the basin and comparable to that of the biggest modern-day river systems, which are supplied by tectonically active orogens; (2) the Middle Triassic sediment load was significantly lower but still comparable to that of the top 10 largest modern rivers; (3) during the Upper Triassic, sediment load increased again in the Carnian; and (4) there is a large mismatch (70%) between the modeled and estimated sediment load of the Carnian. These results are consistent with the Triassic Greater Barents Sea Basin succession being deposited under the influence of the largest volcanic event ever at the Permian-Triassic boundary (Siberian Traps) and concurrent with the climatic changes of the Carnian Pluvial Event and the final stages of the Northern Ural orogeny. They also pro-vide a better understanding of geodynamic impacts on sedimentary systems and improve our knowledge of continental-scale sediment transport. Finally, the study demonstrates bypass of sediment from the Ural Mountains and West Siberia into the adjacent Arctic Sverdrup, Chukotka, and Alaska Basins in Late Carnian and Late Norian time.
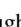
INTRODUCTION

Variations in amounts of sediment supplied to sedimentary basins and continental margins through geological time reflect variations in source-area tectonics and climate (Fig. 1) (Galloway et al., 2011; Braun et al., 2014). In general, areas with high-relief, large source areas, wet and warm climate, and easily erodible lithologies supply more sediment than areas where these factors are lower (Syvitski and Milliman, 2007). Sediment supply rates in ancient sedimentary basins can be determined using, e.g., seismic data, well control, and biostratigraphic dating. In addition, these data are often used to constrain tectonic, climatic, and sedimentary evolution of the sedimentary basin and its hinterland. The configuration of the Arctic basins in the Mesozoic has been a topic of debate (Embry, 1993; Miller et al., 2013; Shephard et al., 2013; Anfinson et al., 2016; Doré et al., 2016; Nikishin et al., 2019; Døssing et al., 2020), and in particular, sediment routing systems and sediment provenance are controversial (Miller et al., 2006; Fleming et al., 2016; Klausen et al., 2017; Hadlari et al., 2018; Sømme et al., 2018). Sediments from the Urals, West Siberia, or Taimyr are thought to have been transported long distances across the Arctic in the Late Triassic (Miller et al., 2018; Sømme et al., 2018), but the tectonic evolution in the source area, the location of sedi-ment sources, and the mechanism of sediment transport across vast distances remains unclear.

The Greater Barents Sea Basin includes the Barents Sea, Svalbard, NW Kara Sea, and Franz Josef Land (Fig. 2), and Arctic Russia and Norway lie adjacent to these basins and act as long-lived sources of sediment that have evolved through geological time. The basin contains a thick and extensive sedimentary succession (up to 4.5 km over an area of 2.5×10^6 km^2) (Fig. 3), which records the evolution of these sediment sources. Here, stratigraphic age and sediment transport directions are well-known due to (1) an abundance of publicly available core, well, and seismic reflection data; (2) well-imaged clino-forms and fluvial channels (Glørstad-Clark et al., 2010; Klausen et al., 2015; Eide et al., 2018a; Rossi et al., 2019); (3) good palynostratigraphic time control (Vigran et al., 2014; Paterson and Mangerud, 2019); (4) a long history of research; and (5) regionally recognizable seismic marker surfaces (flooding surfaces) with time-strati-graphic significance (Gilmullina et al., 2021). This makes it possible to determine the amount of sediment supplied to the basin through time and the overall directions of sediment transport.

Previous studies provided insights into the source of siliciclastic material based on petrog-raphy of sandstones (Mørk, 1999; Fleming et al., 2016; Flowerdew et al., 2019), detrital zircons (Omma et al., 2011; Bue and Andresen, 2014; Fleming et al., 2016; Klausen et al., 2017; Klausen et al., 2019; Khudoley et al., 2019; Haile et al., 2021; Flowerdew et al., 2019), chrome spinel (Harstad et al., 2020), and seis-mic data (Glørstad-Clark et al., 2010; Gilmul-lina et al., 2021). However, these studies have not attempted to study the evolution of the source areas through the entire Triassic. None have investigated how the sediment budget in

Albina Gilmullina ⓘ http://orcid.org/0000-0001-6187-9029; Tore Grane Klausen ⓘ https://orcid.org/0000-0003-2524-512X; Valentina Rossi ⓘ https://orcid.org/0000-0002-2853-6160; Christian Haug Eide ⓘ https://orcid.org/0000-0003-4949-9917

[†]Corresponding author: albina.gilmullina@uib.no.
[§]tore.klausen@gmail.com; agdore@googlemail.com; valentina.marzia.rossi@gmail.com; a.suslova@oilmsu.ru; christian.eide@uib.no.
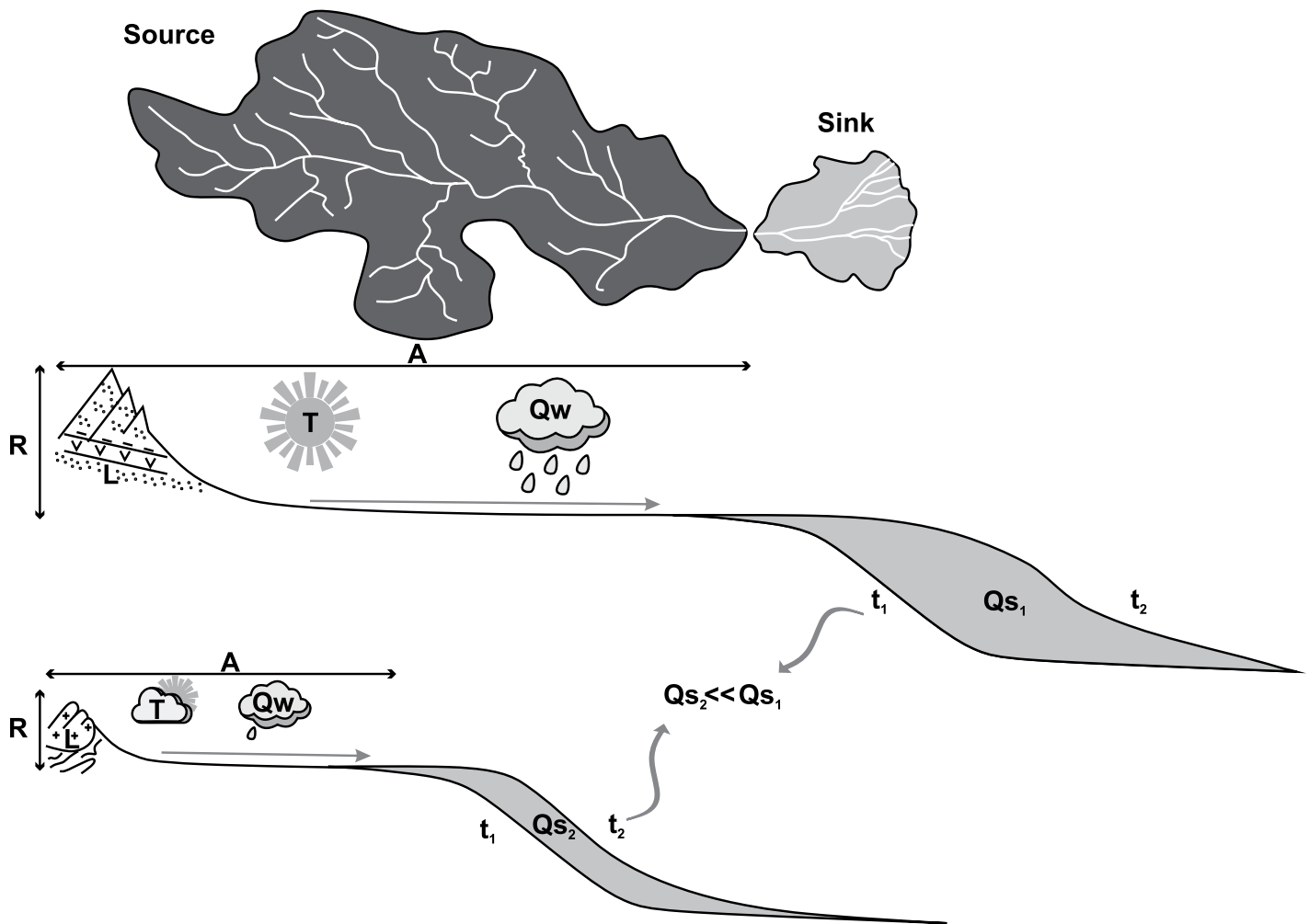
Figure 1. Scheme of the source-to-sink system with main parameters used in the LQART Monte Carlo simulation model is shown; modified from Helland-Hansen et al. (2016) and Zhang et al. (2018a). L—lithology; Q_w—water discharge; A—catchment area; R—maximum catchment relief; T—catchment-averaged temperature; Q_s—sediment discharge.

the basin developed through time. Our analysis of the subsurface data from the Greater Barents Sea Basin presented here shows that enormous amounts of sediment were supplied to the basin, and the sediment supply rates varied significantly through time. These sediments were formerly interpreted to have been supplied from the Urals (Bergan and Knarud, 1993), but recently more diverse source areas have been suggested for parts of the basin in the Late Triassic, such as Taimyr (e.g., Fleming et al., 2016; Harstad et al., 2020), West Siberia, the Central Asian Orogenic Belt (Sømme et al., 2018; Khudoley et al., 2019), and Novaya Zemlya (Zhang et al., 2018b; Klausen et al., 2017). Significant uncertainty about the evolution, timing, and relative magnitude of the tectonic evolution of these sources remains, and that will be evaluated in this contribution.

The aims of this paper are fourfold:

(1) To determine sediment load (mass of sediment supplied to the basin per year) for each Triassic-age stratigraphic unit in the Barents Sea and compare it to sediment load in modern and ancient systems;

(2) To use the BQART approach (Syvitski and Milliman, 2007; Sømme et al., 2009) to assess possible scenarios for how the source areas surrounding the Greater Barents Sea Basin evolved and determine which geographical areas are realistic as sediment sources areas;

(3) To link the changes in sediment load and catchment parameters to tectonic and climatic events in the source area; and

(4) To evaluate models for understanding the evolution of continental-scale, source-to-sink systems (Fig. 1) in deep time in general.

GEOLOGICAL SETTING

From the beginning of the Triassic, the Greater Barents Sea Basin experienced rapid and poorly understood subsidence (e.g., Gac et al., 2012, 2016), which coincided with deposition of up to 4.5 km of mudstone-dominated clinoform packages (Fig. 3). Stratigraphic units are defined by discrete maximum flooding surfaces that can be traced across the entire basin based on seismic data and tied to core and well data dated by biostratigraphy (Gilmullina et al., 2021). These deposits prograded from the SE toward the NW (Fig. 4) (Glørstad-Clark et al., 2010; Klausen et al., 2015, 2018; Gilmullina et al., 2021) across the entire basin and share relatively similar provenance characteristics. They are commonly interpreted to have been sourced from the Urals with minor contributions from different nearby areas (Mørk, 1999; Bue and Andresen, 2014; Fleming et al., 2016; Flowerdew et al., 2019; Khudoley et al., 2019). This interpretation implies that a river system must have run along the western part of the Ural orogen along the western foreland basin and supplied
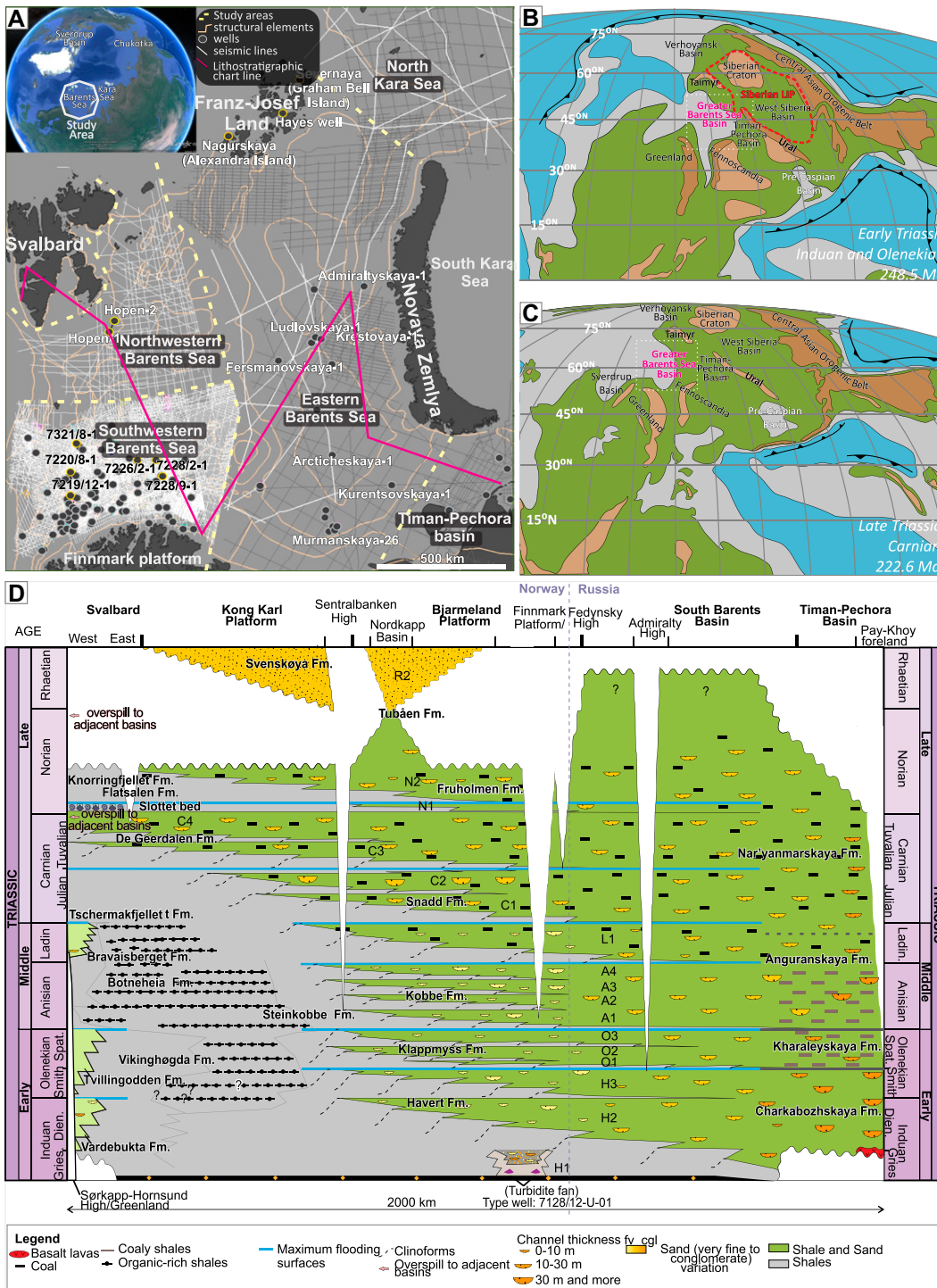
Figure 2. The entire Greater Barents Sea Basin is shown. (A) The six geographic regions and all seismic and well data available from Gilmullina et al. (2021); (B–C) regional overview location maps of the Greater Barents Sea Basin and paleogeography in the early Induan (Early Triassic) and Carnian (Late Triassic) from Scotese and Wright (2018); (D) lithostratigraphic correlation of the Triassic with different parts of the Greater Barents Sea Basin from Gilmullina et al. (2021).

sediments to the Greater Barents Sea Basin, which lay at the end of this foreland basin (Fig. 5). This is similar to the modern Ganges River, which runs along the Himalayan orogen through the southern foreland basin and overspills sediments to the Bay of Bengal, where the foreland basin ends.

Marked progradation caused by great sediment supply in the Triassic Greater Barents Sea Basin occurs in the Induan (Early Triassic) and the Carnian. (Late Triassic) (Figs. 3–4) (Glørstad-Clark et al., 2010; Klausen et al., 2015; Gilmullina et al., 2021). The large-scale progradation in the Induan is not coincident with any contractional orogenic event in the Urals (Puchkov, 2009), and it has therefore been suggested that this progradation was caused by regional tectonic uplift resulting from activity in the Siberian Traps Large Igneous Province (Figs. 4–5) (Eide et al., 2018a). The Carnian progradation coincides both with the Carnian Pluvial Event and the re-initiation of contraction in the Northern Urals (Klausen et al., 2015; Gilmullina et al., 2021). During the Middle Triassic, sedimentary packages are thin and show short progradational distances (Glørstad-Clark et al., 2010; Gilmullina et al., 2021). No particular
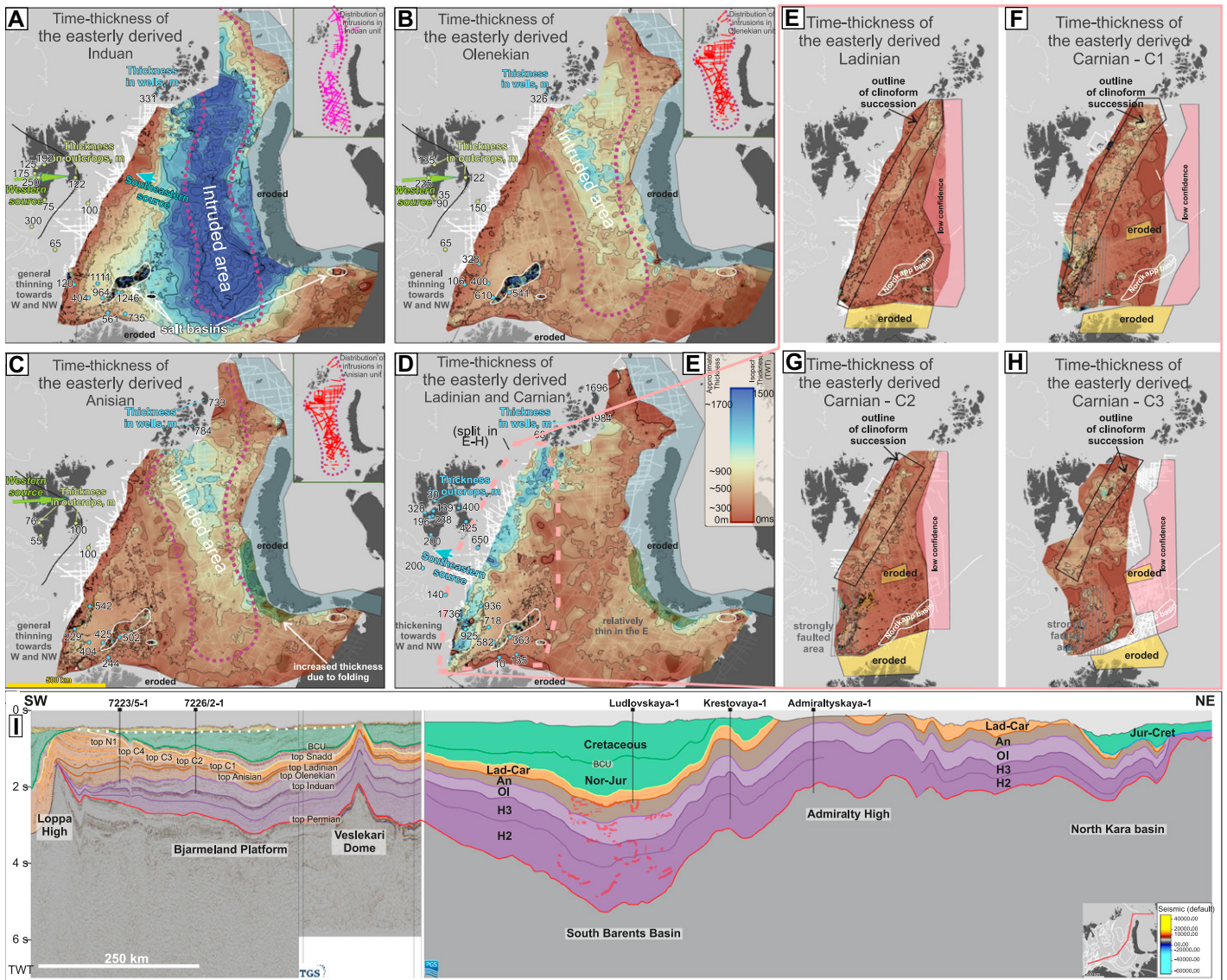
Figure 3. (A–H) Time-thickness maps show the main stratigraphic units. The color scale, from Crameri (2018), is equal for the different maps. (I) A regional composite seismic line from the Loppa High via the Admiralty High to the Kara Sea from Gilmullina et al. (2021). Note that the thickness maps and the seismic line indicate that that the prograding easterly stratigraphic units were contained within the Greater Barents Sea Basin until the Carnian (A–C, E, and I) and prograded beyond the Greater Barents Sea Basin from the C2 (G–I).

tectonic events are recorded in the source area at this time. Sedimentation rates in the Norian are difficult to ascertain due to extensive erosion underneath a regional unconformity that developed in the basin during the Rhaetian (Fig. 2) (Müller et al., 2019).

Eastern Source Evolution

Based on sediment transport directions derived from clinoform directions (Glørstad-Clark et al., 2010; Gilmullina et al., 2021) and fluvial channel-orientations (Klausen et al., 2014, 2015, 2019; Eide et al., 2018a), it is clear that most of the Triassic sediments sup-

plied to the Barents Sea Basin are sourced from the southeast (Fig. 4). Sediment supplied by the Eastern Source comprises 99% of all the Triassic sediments that can be mapped in seismic data in the Greater Barents Sea Basin. The Eastern Source in this study is very extensive and broadly defined to include the uplands east and southeast of the Barents Sea and comprises areas such as the Urals (Mørk, 1999) with contributions from Taimyr (Fleming et al., 2016) and the Kara Sea (Daragan-Sushchova et al., 2014), West Siberia (Sømme et al., 2018; Khudoley et al., 2019), East Siberia, and the Central Asian Orogenic Belt (Sømme et al., 2018; Figs. 4–5).

METHODS AND DATA

Workflow to Determine Estimated Sediment Load

To calculate the amount of observed sediment supplied to the basin per year (sediment load) throughout the Triassic, the following workflow was used: (1) the time-thickness of each stratigraphic time unit (corresponding roughly to second-order sequences, as defined in Gilmullina et al., 2021) is determined using seismic data in a data set of 3238 2-D seismic lines covering 1,700,000 km², a set of 3-D seismic data sets from the SW Barents Sea, and 257 wells with wireline
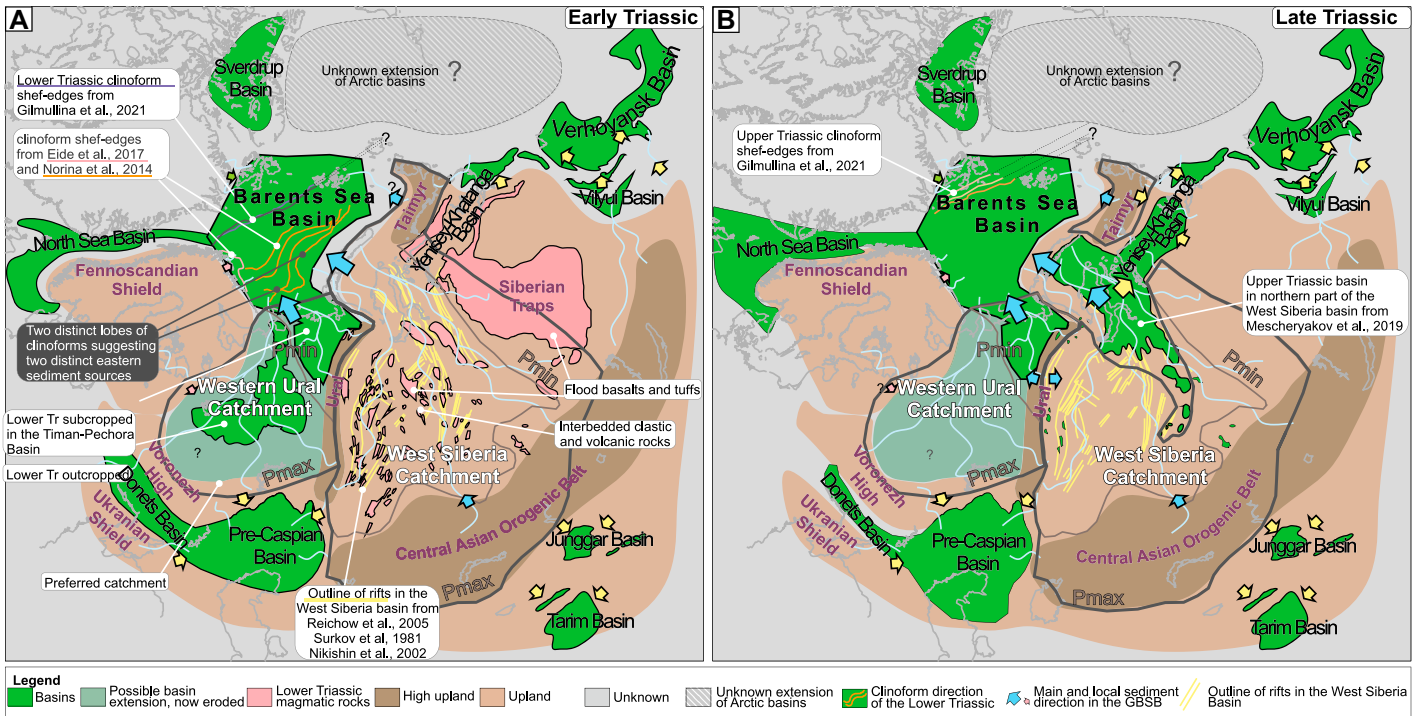
Figure 4. The extents of the Western Urals and West Siberian Catchments, which developed in the eastern sediment source, are shown in (A) the Early Triassic and (B) the Late Triassic. The main sediment directions and locations of the basins and uplands are modified from Nikishin et al. (1996, 2002, 2010), Reichow et al. (2009), Bukina and Yanochkina (2011), Embry (2011), Li et al. (2013), Norina et al. (2014), Wang et al. (2017), Eide et al. (2018a), Meshcheryakov et al. (2019), and Gilmullina et al. (2021). GBSB—Great Barents Sea Basin.

logs and biostratigraphic data across the Greater Barents Sea Basin (Gilmullina et al., 2021); (2) the top and bottom surface of each time unit is depth-converted using a time-depth relationship determined from checkshot data; (3) mass of each time-unit is determined by multiplying the thickness map with a density map created using a density-depth relationship determined from density-logs from Greater Barents Sea Basin
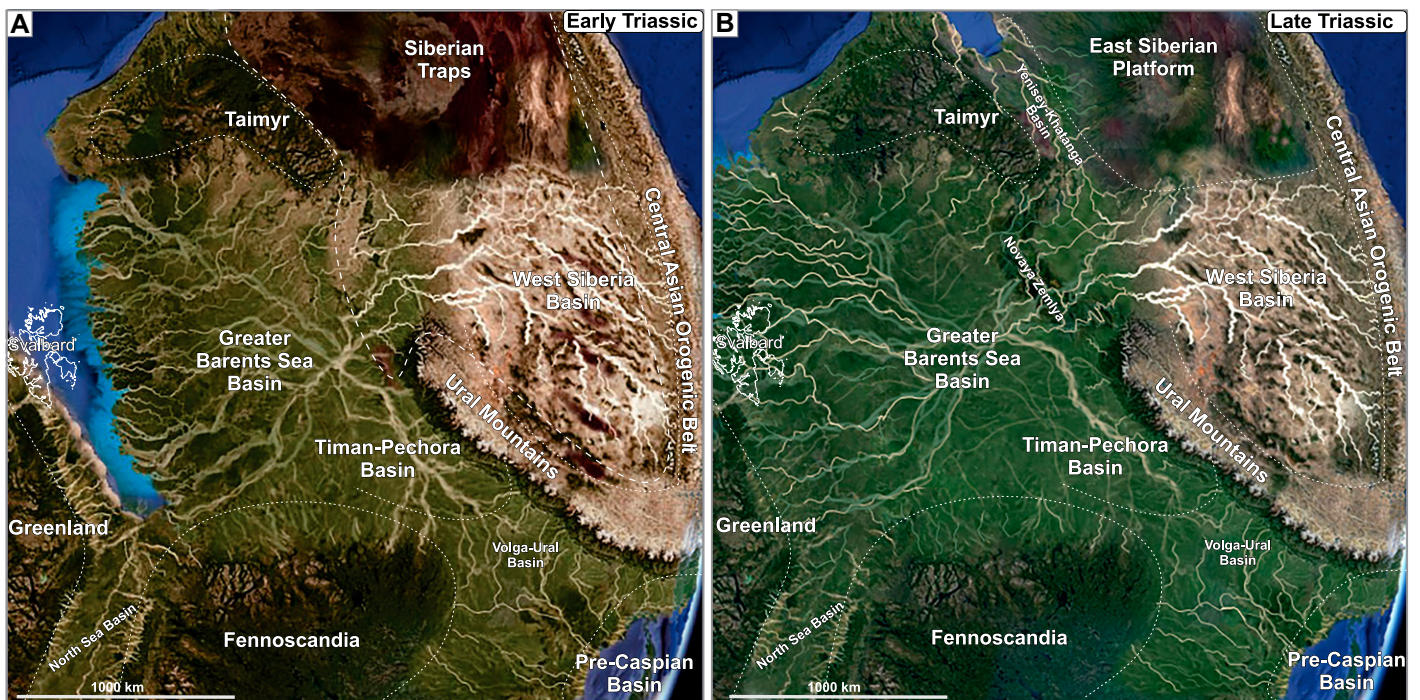

Figure 5. (A) Early Triassic and (B) Late Triassic paleogeographic reconstructions are shown (from Google Earth Pro 7.1.2.2041).

Geological Society of America Bulletin

exploration wells ($\rho = 116{,}51\ln(z) + 1655{,}4$ where ρ is in kg/m^3 and z is depth in meters); (4) total mass of each time unit is divided by the duration of each time unit determined by biostratigraphic data (Paterson and Mangerud, 2019; Gilmullina et al., 2021) and by using the timescale from Ogg et al. (2014), which gives sediment load in megatons per year (MT/yr).

Reconstructed Sediment Load

The observed masses of sediment clearly underestimate the real mass of sediment supplied during the Triassic because of (1) post-depositional erosion (Müller et al., 2019), (2) bypass of sediments to adjacent basins (Klausen et al., 2015), and (3) deposition of sediment in areas without seismic coverage (Gilmullina et al., 2021). Some mass was also added after deposition because of the (4) incursion of igneous intrusions in the Northern and Eastern Barents Sea (Polteau et al., 2016; Gilmullina et al., 2021). These factors must be corrected for and addressed to provide an accurate picture of sediment supplied to the basin from the eastern sediment source. From here on, the corrected observed sediment load will be called the *estimated sediment load*.

Post-Depositional Erosion

The Triassic deposits in the Greater Barents Sea have been subject to post-depositional erosion especially toward basin margins (north of Fennoscandia, Novaya Zemlya, NW Svalbard, and the Kara Sea) and on the Sentralbanken High.

Svalbard was affected by the uplift and partial erosion of Carnian C3 + 4 and Norian N1–2 deposits (Fig. 2) and complete erosion of the Triassic in the northern part of the archipelago. To determine the original Upper Triassic volumes across Svalbard, available thicknesses from outcrop data were extrapolated to areas where Triassic deposits are eroded.

Two major tectonic events resulted in regional erosional unconformities during the Triassic-Jurassic and Cenozoic that led to localized erosion of the upper parts of the Triassic deposits and erosion to depths of 0 m to 2.5 km from the South Barents Sea Basin to Loppa High, Svalbard, and the North Kara Platform (Gilmullina et al., 2021; their fig. 14). Novaya Zemlya was a basin in the Early Triassic (Gilmullina et al., 2021; Haile et al., 2021) and probably accumulated Triassic deposits at the same thickness as is found in the adjacent South Barents Sea Basin and Admiralty High. During the Late Triassic, Novaya Zemlya was affected by contraction and uplift, and the exact timing of this will be discussed below. For the restorations of eroded sediment volumes, thickness maps adjacent to Novaya Zemlya were extrapolated into the now-eroded areas (Figs. 3 and 6).

Deposits that were eroded in the Kara Sea and Finnmark Platform were not restored due to the unknown distribution and continuation of the Triassic units into these areas. The eroded volumes along Fennoscandia are assumed to be small because this area was close to the southern source (see Eide et al., 2018a). The missing volumes in the Kara Sea are unconstrained, and no attempt has been made here to correct for the missing masses.

Sediment Bypass to Adjacent Basins

Seismic data show that basinward-dipping clinoform surfaces continue as far as data coverage goes toward the west, northwest, and north in the Greater Barents Sea Basin (Fig. 3I; Gilmullina et al., 2021). The great thickness (1700 ms TWT, ~1800 m) of the clinoform package that abruptly ends toward the basin's margins (Fig. 3) strongly suggests the Triassic sediments prograded beyond the available data set and the present-day Greater Barents Sea Basin. Throughout the Triassic, there are three areas where bypass of the prograding sedimentary package could occur: (1) north of Franz-Josef Land and the Sant Anna Basin throughout the Triassic, (2) along the Atlantic margin from the Ladinian, and (3) along the northern and western margins of the Greater Barents Sea Basin and NW of Svalbard during the Late Carnian and Late Norian (Gilmullina et al., 2021; Fig. 2).

The amount of sediment bypass to adjacent basins is highly uncertain and therefore is treated as an unknown in this contribution, but simple estimates are presented below. These estimates were made by extrapolating thickness maps of
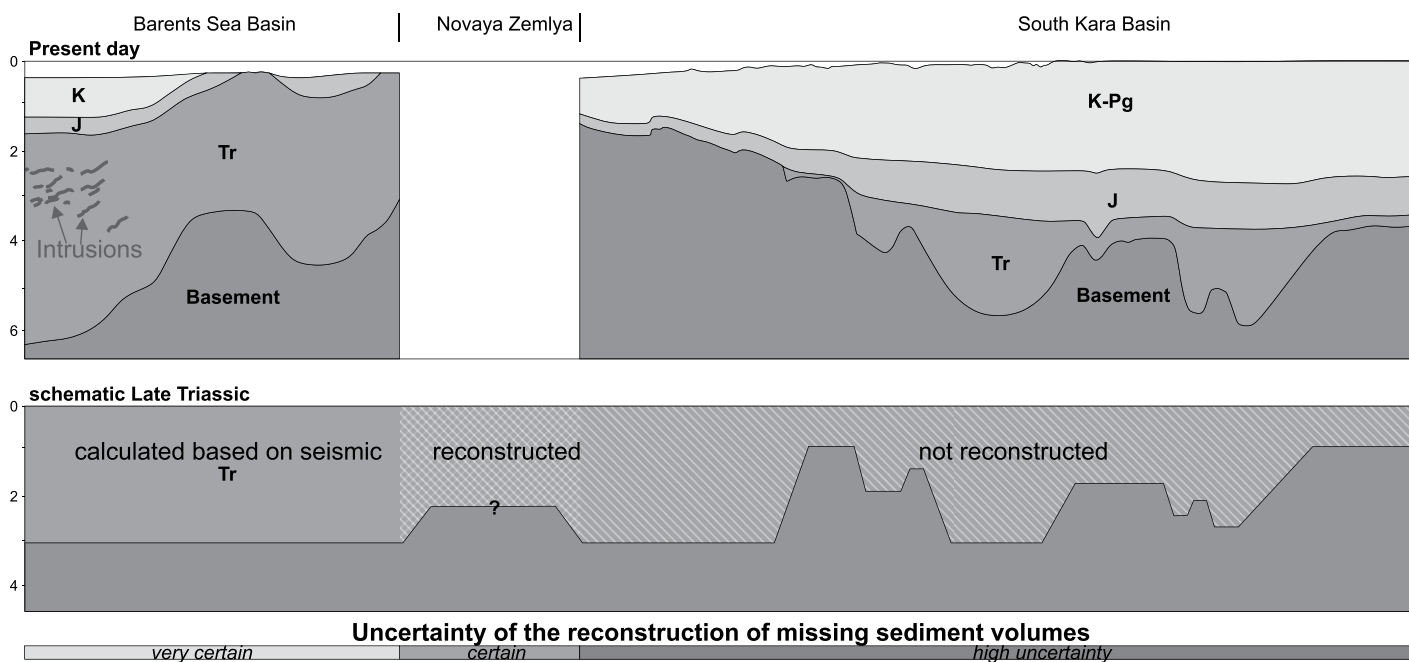

Figure 6. Late Triassic paleo reconstruction shows geological cross section through the Eastern Barents Sea, Novaya Zemlya, and South Kara Basin. Note the amount of sediment possibly eroded from Novaya Zemlya and the western part of the South Kara Basin.

the stratigraphic units as far as the well-constrained NW pinch-out into the basins that have since rifted apart and are now offset (Fig. 3).

Bypass of sediment out of the Greater Barents Sea Basin is based on observations of clinoforms prograding out of the basin (Fig. 3I). We do not believe that significant additional loss of sediment from the basin occurs in the form of advecting plumes or longshore drift because (1) little evidence of strong wave energy is observed in the basin (Klausen et al., 2016), which results in minimal sediment transport as longshore drift; (2) the Greater Barents Sea Basin is very large (1200 ×1800 km) and gives us a great opportunity to preserve plumes and sediment transported by potential longshore drift within the basin; (3) clinoforms are well-imaged and do not show typical contourite geometries; and (4) bottom sets in the basinal areas are very thin, which indicates that minimal clastic sediment was transported great distances.

Deposition in Areas without Seismic Coverage

On the Svalbard Archipelago, the easterly-derived Upper Triassic De Geerdalen Formation deposits belong to the C3 + 4 unit (Fig. 2), and thicknesses from this unit in outcrops were used to calculate sediment mass on Svalbard (Fig. 3). For restoration on Franz Josef Land, trends from thickness maps for each unit (Fig. 3) were used to extrapolate thicknesses into this area. These results were calibrated with thicknesses from the three wells drilled in the archipelago (Dypvik et al., 1998).

The western margin of the Greater Barents Sea Basin was affected by the opening of the Atlantic Ocean, and as a result, the Carnian-Norian deposits are strongly faulted and buried under a thick package of Cretaceous and Paleogene deposits (Fig. 3) that makes them impossible to interpret confidently in seismic data. Therefore, based on the thickness map and distribution of the units, 25% (Carnian units C1 and C2) and 35% (unit C3 + 4) of total mass was extrapolated in this area to reconstruct the minimum mass of buried sediments.

Removal of Igneous Intrusions

Based on studies in East Greenland (Eide et al., 2017) and the Faroe-Shetland Basin (Mark et al., 2019), the presence of layer-parallel mafic igneous intrusions commonly results in a ~10% increase in thickness of the stratigraphic package. Ten percent of the sedimentary volume was therefore subtracted in the areas in the N and E Greater Barents Sea Basin for the stratigraphic units with abundant igneous intrusions (Havert, Klappmyss, and Kobbe Formations) (Fig. 6; Polteau et al., 2016; Gilmullina et al., 2021).

Key Uncertainties

The seismic interpretations, sediment transport directions, and thicknesses in two-way time of the different Lower and Middle Triassic stratigraphic units are highly certain in most parts of the Greater Barents Sea Basin because of good imaging and a simple basin structure (Fig. 3). For the Carnian, the different stratigraphic units cannot be distinguished in the Russian parts of the basin because of little lithological contrast (Fig. 3I), and the Russian portion of the sediment volume is assigned to the different time units in a schematic way (25% to each time unit, which reflects continuous subsidence). The Norian sediment volumes are highly schematic and based on preserved thicknesses in areas of little erosion.

There are some key uncertainties in calculating the masses of stratigraphic units. (1) Parts of the basin, such as the Kara Sea, are up to 800 km from any wells (Fig. 2A), and (2) the deep parts of the basin are not sampled by any wells (Fig. 3I). The uncertainties in the choice of density-depth and velocity-depth curves are, however, small compared to the uncertainties in the BQART modeling. Durations of the Lower and Middle Triassic time units are fairly well constrained (Vigran et al., 2014; Ogg et al., 2014), which leads to good controls on the sediment loads for these time periods. The different Carnian and Norian time units (C1–4) are poorly constrained, and a conceptual time model for these units is chosen here (Fig. 2D). However, changes to this time model would only change the magnitude of sediment load of the different Carnian periods. In sum, this leads to relatively good control of sediment supply in the Lower and Middle Triassic, somewhat good control of sediment supply in the early Carnian, and poor control of sediment supply in the Late Carnian and Norian.

BQART Model and Input Variables

Equation

Syvitski and Milliman (2007) created an empirical model, the BQART model, which explains 96% of the variability of suspended sediment load in a database of 488 modern rivers. In this contribution, we apply this model to investigate the properties of the catchments that supplied sediments to the Greater Barents Sea Basin in the Triassic (Fig. 1). During the Triassic greenhouse (Winguth et al., 2015), catchment-averaged temperatures of the eastern sediment source of the Greater Barents Sea Basin must have been higher than 2 °C, and the catchment cannot have been affected by human activity or glaciations at a scale that would influence these calculations (see equation 9 in Syvitski and

Milliman, 2007). The factor B in the BQART-equation, which includes anthropogenic influence, glaciers, and lithology, thus simplifies to lithology alone. We assume that the sediment load from the catchments supplying sediment to the Triassic Greater Barents Sea Basin can be predicted using the following equation (here called the LQART model):

$$Q_s = \omega L Q_w^{0.31} A^{0.5} R T \qquad (1)$$

where Q_s is sediment discharge (10^6 t/yr), ω is an empirical constant ($\omega = 0.0006$), L is a variable for bedrock erodibility (with extremes of 0.5–3 for hard metamorphic/plutonic bedrock lithologies and erodible loess lithology, respectively), Q_w is annual water discharge (km^3/yr), A is catchment area (km^2), R is maximum catchment relief (km), and T is the long-term, basin-averaged temperature (°C).

Because the sediment load supplied from a catchment is strongly related to the parameters of the catchment (lithology (L), water discharge (Q_w), catchment area (A), maximum catchment relief (R), and catchment-averaged temperature (T); Syvitski and Milliman, 2007), the sediment load variations can be used to study how the catchments evolved through time. Because five different catchment parameters with great uncertainties are considered, unique solutions to Equation 1 do not exist. Instead, we vary the catchment parameters within geologically realistic bounds (see below, Fig. 7), perform multiple calculations (Monte Carlo simulation), and investigate whether the observed and estimated sediment loads fit the sediment load values calculated from the LQART model. Such estimates, especially in ancient deposits, have a large uncertainty (e.g., Nyberg et al., 2021). The Monte Carlo simulations display the distribution of possible values for different scenarios, and for such tests to be valid, the distributions after Monte Carlo simulation must be clearly different (i.e., not overlapping). The main objectives of the LQART modeling are as follows.

(1) To test if the Western Urals Catchment could have supplied enough sediment to create the observed sediment loads alone or if the observed sediment loads also require a contribution of other catchments such as West Siberia and the Central Asian Orogenic Belt.

(2) To investigate the reasons for the large variations in sediment loads in the Greater Barents Sea Basin during the Triassic (Fig. 8).

(3) To investigate the magnitudes of sediment bypass to adjacent sedimentary basins.

Catchment Parameters

Lithology (L). The lithology in a vast catchment must have been variable. The present-day
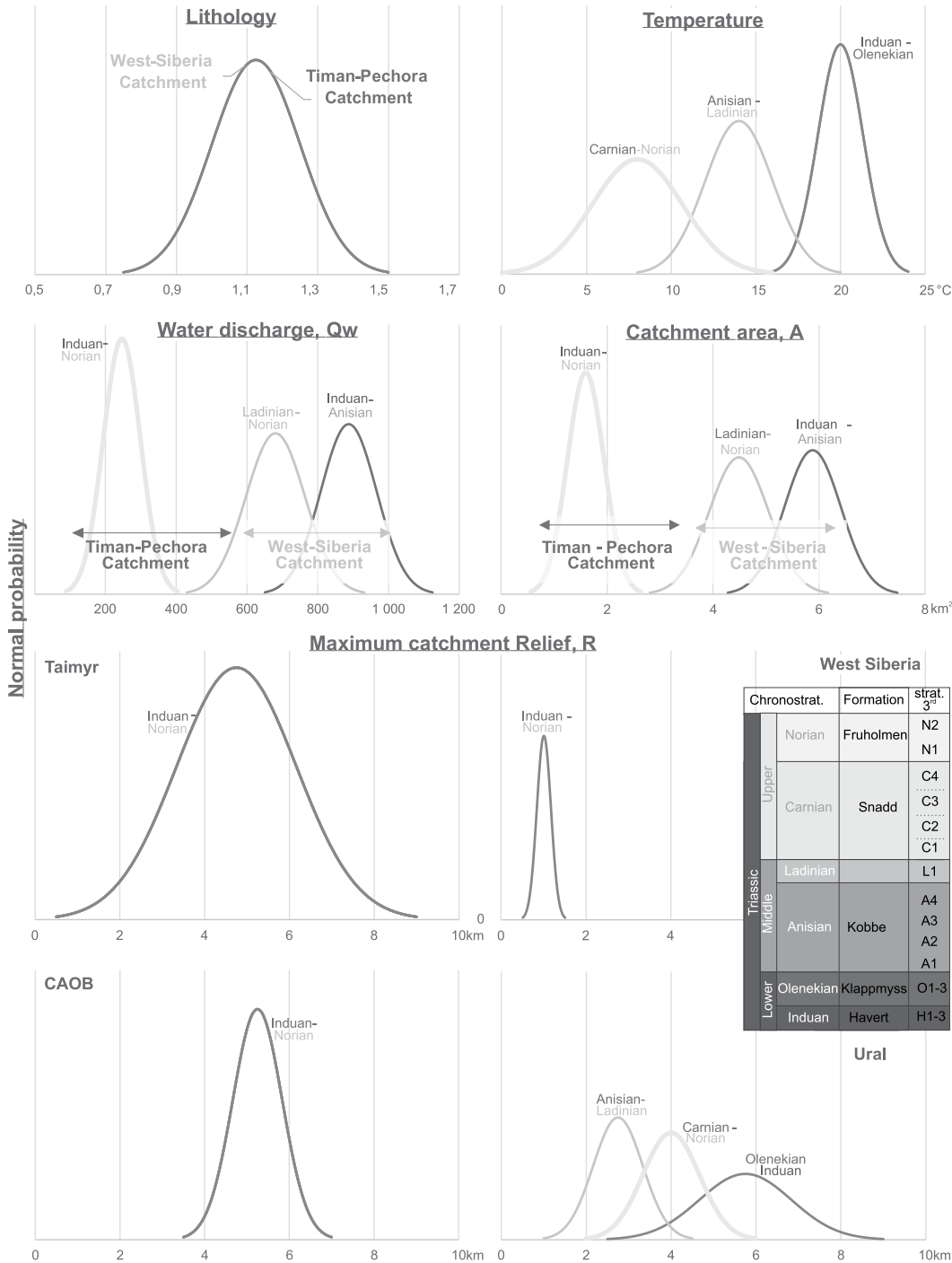
Figure 7. LQART parameters used for the Monte-Carlo simulation model are shown (for more detailed description, see the BQART model and input parameters). CAOB—Central Asian Orogenic Belt.

geological map of Russia shows that the Uralian thrust belt consisted of a variety of clastic, igneous, and metamorphic lithologies; in addition, parts of the catchment must have been covered by loose sediment, and if the Siberian Traps were an additional source, volcanic terrains were also drained (Petrov et al., 2012, 2016, https://vsegei.ru/ru/info/webmapget/). This leads to an overall catchment-averaged lithology value of 1, which is classified as "mixed or carbonates, volcanics" (sensu Syvitski and Milliman, 2007). The other possible catchment areas were also vast and consisted of diverse lithologies and were also assigned a lithology value of 1. To provide realistic bounds to add variation for the Monte Carlo simulation, a normal distribution from 0.75 to 1.5 has been assigned (Fig. 7).

Temperature (T). Catchment-averaged temperature is specified for the Lower (251.9–247.2 Ma), Middle (247.2–237 Ma), and Upper (237–201.3 Ma) Triassic separately and is assigned to a normal distribution within the distinct range 16–24 °C, 8–20 °C, and 0–12 °C, respectively, that captures the relevant uncertainty range but also captures the Early Triassic greenhouse and overall Triassic climatic cooling (Fig. 7; Scotese and Moore, 2014). Globally, the Triassic was generally hot and arid (Sellwood and Valdes, 2006) but with geographic and temporal variations.
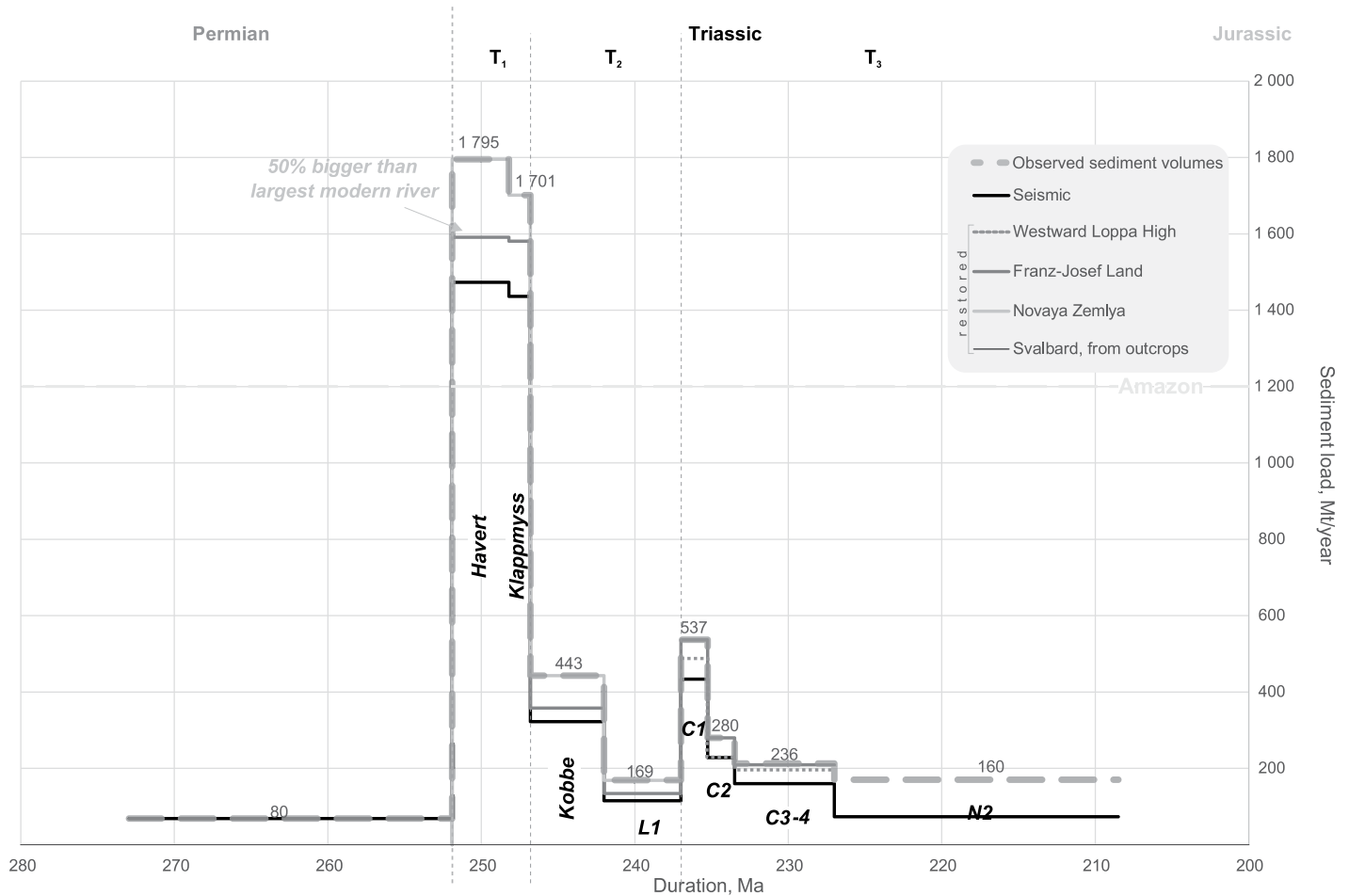
Figure 8. Sediment load is estimated for each stratigraphic unit in the Greater Barents Sea Basin from seismic data and shown for post-Triassic erosion. Note the dramatic increase in sediment volume at the Permian–Triassic boundary and Middle–Late Triassic and decrease in the Middle and Late Triassic.

Water discharge (Q_w). Water discharge of ancient rivers and catchments is difficult to estimate, but general considerations can be made and implemented by correlating water discharge (Q_w), catchment area (A), and catchment humidity (k, m) (Eide et al., 2018b)

$$Qw = k^*A^m \qquad (2).$$

Rapid global warming just after the Permian-Triassic boundary, probably partly caused by an eruption of the Siberian Traps (Sun et al., 2012), led to a dominantly semi-arid climate in the Early Triassic in the study area as indicated by red-colored paleosols and redbeds and the global absence of coals (Chumakov and Zharkov, 2003; Péron et al., 2005; Nystuen et al., 2014; Eide et al., 2018b). Cooling and normalization of the temperatures occurred in the Middle Triassic (Sun et al., 2012) and coincided with deposition of organic-rich shales in the NW Barents Sea and across the Arctic (Grasby et al., 2020). The

Late Triassic was characterized by humidification with short warming phases (Fig. 7) (Sellwood and Valdes, 2006, Trotter et al., 2015). This evolution was implemented in the models using coefficients and exponents corresponding to semi-arid conditions during the Early Triassic and humid conditions during the remainder of the Triassic.

Catchment area (A). Certain distinct areas could possibly have contributed to filling the Greater Barents Sea Basin in the Triassic (Fig. 5). We investigate which of these geographical areas could have been part of the catchment and contributed sediment to the Greater Barents Sea Basin by using their respective areas in different LQART models: West Uralian foreland, West Siberia with the eastern Urals and western East Siberia, northern Central Asian Orogenic Belt, and Taimyr (Fig. 4).

Clinoform directions and fluvial channel geometries in the Greater Barents Sea Basin constrain the sediment transport directions to be

broadly from the east. Consistent northwestern sediment transport dominates throughout the Triassic from the Induan to Norian, and a linear clinoform front stretches across the entire Greater Barents Sea Basin (Fig. 3; Glørstad-Clark et al., 2010; Gilmullina et al., 2021) with fluvial channels oriented toward the northwest (Klausen et al., 2015). However, during the earliest Induan, at the very early stages of infill, the clinoform belt shows two clear protrusions with one to the west of the Urals and one to the east of the Urals (Fig. 4, orange lines). This critical observation strongly suggests that the sediments in the Greater Barents Sea Basin were supplied not only from the Western Urals from the side of Timan-Pechora Basin but also from the West Siberian Basin (Fig. 5). A northwest orientation of the clinoform belt across the Greater Barents Sea Basin agrees better with sediment input from multiple sources around the eastern margin of the basin rather than one sediment input point at the north end of the Western Urals. This also agrees

well with the overall geometry of the Triassic deposits in the South Kara Sea and West Siberian Basins, where a series of narrow, N-S–trending (possibly rift) basins occurs (Fig. 4; Nikishin et al., 2002; Daragan-Sushchova et al., 2014). Such basins could have funneled sediments from West Siberia and even the Central Asian Orogenic Belt northward toward the Kara Sea and Barents Sea (e.g., Miller et al., 2013). The maximum extent of the Lower Triassic Western Urals Catchment was limited to the east by the Ural Orogenic Belt, the Baltic shield to the west, the Voronezh high to the southwest, and the uplifted part of the Volga-Ural Basin to the south (Fig. 4; Nikishin et al., 1996, 2002). The Western Urals Catchment could have increased to its maximum extent in the Late Triassic due to uplift of the Northern Urals and Novaya Zemlya (Puchkov, 2009).

The maximum extent of the Lower–Middle Triassic (Anisian) West Siberian Catchment includes three areas: West Siberian Basin with the western part of the Siberian Platform, the northern Central Asian Orogenic Belt to the south, and Taimyr to the north. The West Siberian Basin was composed of a rift valley system where rift shoulders were a local sediment source and grabens acted as transportation pathways (Saraev et al., 2011). By the end of the Anisian, magmatic activity related to the Siberian Traps ceased in the West Siberian Basin, and the northern part of the basin started to subside (Meshcheryakov and Karaseva, 2010; Sømme et al., 2018); the West Siberian Catchment decreased in size during Ladinian–Norian time (Fig. 4) due to this newly formed basin.

A large catchment extent is supported by detrital zircon studies, which indicate that the Urals (Omma, 2009; Bue and Andresen, 2014; Klausen et al., 2017; Klausen et al., 2019; Flowerdew et al., 2019), Taimyr (Fleming et al., 2016), West Siberia, and the Central Asian Orogenic Belt (Tevelev, 2013; Khudoley et al., 2019; Soloviev et al., 2015) all could have contributed.

In a study of the Carnian delta systems of the Greater Barents Sea Basin by Klausen et al. (2019), it was assumed that uplift in Novaya Zemlya (e.g., Haile et al., 2021; Gilmullina et al., 2021) created a barrier to sediment supply from West Siberia beginning in the Carnian. This is not necessarily the case, because young detrital zircons in the easterly derived sediments (e.g., Fleming et al., 2016), combined with channel and clinoform directions (Gilmullina et al., 2021), indicate that sediment supply from West Siberia to the Greater Barents Sea Basin might have continued into the Norian. The External Sierras of the Spanish Pyrenees is an example of an uplifting area where river systems could bypass, as no significant topography was con-

structed as long as easily erodible sediments were uplifted (Lloyd et al., 1998), and this could be a model for how large amounts of sediments could be transported from West Siberia into the Greater Barents Sea Basin. Below, we test whether the Urals alone could have supplied the observed amounts of sediment in the Greater Barents Sea Basin or if the sediment volumes require a larger catchment that would be consistent with drainage in West Siberia.

Maximum catchment relief (R). Relief is assigned to a normal distribution for each of the sub-catchments in the latest Triassic (Fig. 7): (1) Ural, (2) Central Asian Orogenic Belt, (3) West Siberia and part of Siberian Traps, (4) Taimyr, and (5) Novaya Zemlya. Ancient relief is difficult to estimate, and values here are based on a general understanding of tectonic evolution and relief of modern analogues (e.g., Parrish, 1998).

The Ural orogeny was formed because of continent-continent collision around the Carboniferous-Permian boundary and was reactivated around the Permian–Triassic boundary (Leech and Stockli, 2000; Puchkov, 2009). The present-day Himalayas are an example of continent-continent collision today, and maximum relief is close to 9 km. However, as the driver of the topography of the Urals during the Early Triassic reactivation is uncertain, a wide range of possible elevations has been specified for the Early Triassic: 2.5–9 km. The Middle Triassic is associated with less tectonic activity, and a range of 1–4.5 km that corresponds to mountains of medium height has been specified. The Upper Triassic is associated with a new active phase in the northern part that includes Polar Ural, Pay-Khoy (Nikishin et al., 2002), and Novaya Zemlya (Müller et al., 2019), and topography of 2–6 km has been used.

The Central Asian Orogenic Belt (also called the Altaids; Şengör and Natal'in, 1996, 2004) is one of the longest-lived accretionary orogens, and its geological history remains controversial (Wilhem et al., 2012; Xiao et al., 2015). Accretion goes back to the Vendian, when it evolved between Siberia, Gondwana, and the Tarim–North China cratons. Parts of the Central Asian Orogenic Belt were a complex, subduction-related orogen in the Triassic (e.g., Zhang et al., 2009), but no significant variations relevant to the BQART models reported in this paper have been described. Relief is therefore assigned to 3.5–7 km throughout the Triassic.

The West Siberian Basin is located between the Urals to the west, Siberian craton to the east, Kazakhstan upland, and the Altay-Sayan Mountains to the south. The basement of the West Siberian Basin is composed of multiple blocks and arcs of the Kazakh continent and is the result of a collision between the Baltica and Siberia

platforms that concluded during the Permian (Vyssotski et al., 2006). The West Siberian Basin was a magmatically active area that included the Siberian Traps Large Igneous Province, which was associated with regional hotspot-related volcanism (Reichow et al., 2009) and stored large amounts of igneous and volcaniclastic material; relief of 0.5–1.5 km has been specified.

Another proposed sediment source area of the Greater Barents Sea Basin is the Taimyr orogen (e.g., Fleming et al., 2016; Harstad et al., in revision). The Taimyr Orogen resulted from the collision of the Kara terrane and Siberian craton in the Carboniferous to Early Permian (Vernikovsky et al., 2003; Kurapov et al., 2020). Magmatic rocks dated to ca. 250 Ma are widespread in Taimyr and were emplaced either as part of the Siberian traps (Augland et al., 2019) or separately as post-collisional granitoids associated with the Kara Orogen (Vernikovsky et al., 2020). Later, Taimyr experienced Middle–Upper Triassic granite intrusions (Zhang et al., 2018b), and then another major deformational phase took place in the Late Triassic to the earliest Jurassic (Pease, 2011; Ershova et al., 2015; Khudoley et al., 2018). Thus, the relief throughout these events is very uncertain and has been assigned to a wide range of 0.5–9 km throughout the Triassic.

Monte Carlo Simulation

Monte Carlo simulations (MCS) were used to model expected sediment supply from the eastern sediment source using realistic catchment parameters. To do this, we formulated a Monte Carlo simulator in Microsoft Excel (see Supplemental Material S1[1]). The calculations were also verified using two different commercial MSC packages, and all yielded nearly identical results. Input parameters L, Q_w, A, R, and T were specified for each time unit as normal distributions within geologically realistic limits, which were determined using geological maps, tectonic setting of the source area, palaeogeographic reconstructions, modern analogues, and published studies. The MCS iterates 5000 realizations of the LQART model per stratigraphic unit (Fig. 9); the variables in Equation (1) were chosen randomly using the specified probability distributions.

RESULTS

The following section reports the results of estimated sediment load from seismic data,
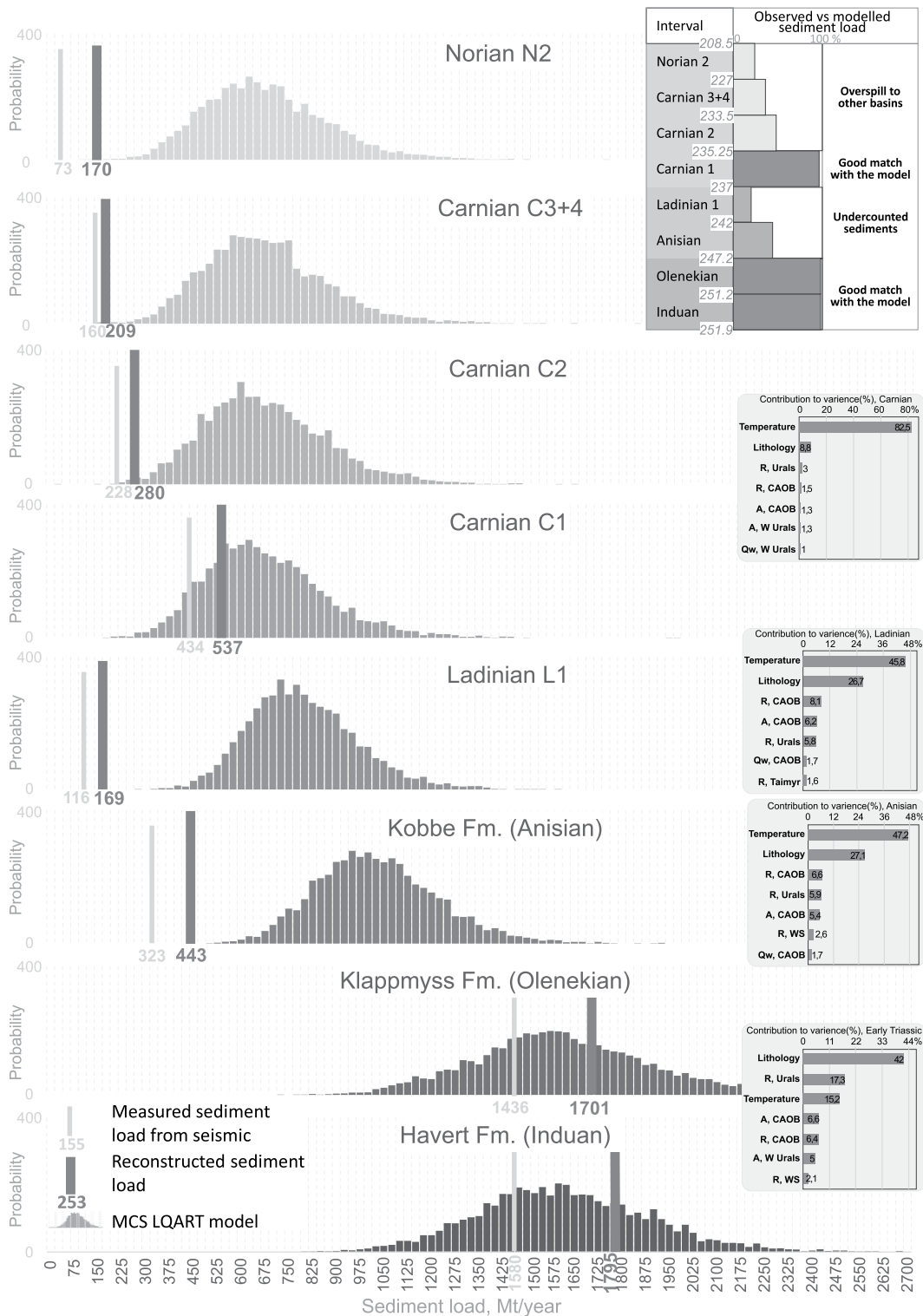
Figure 9. Probability distribution shows sediment supply of the easterly derived Triassic deposits for each stratigraphic unit and position where sediment load (thick dark gray pole) was measured. CAOB— Central Asian Orogenic Belt; MCS—Monte Carlo simulation.

modeling of sediment load using the LQART equation, comparison of results from different methods, and considers which of the many sediment source areas are required to provide the observed amount of sediment in the Greater Barents Sea Basin.

Triassic Sediment Load to the Greater Barents Sea Basin

Analysis of subsurface and outcrop data indicates that ~1.4×10¹⁹ kg of sediment was supplied from the eastern sediment source to the

Greater Barents Sea Basin during the Triassic (Tables 1 and S1; see footnote 1). The source of these sediments in the east is verified by provenance data (Bue and Andresen, 2013; Flowerdew et al., 2019), clinoform and river channel directions (Glørstad-Clark et al., 2010; Klausen

TABLE 1. SEDIMENT LOAD PARAMETERS FOR THE DIFFERENT
STRATIGRAPHIC UNITS IN THE GREATER BARENTS SEA BASIN

Unit	Mass (kg)	Volume (km³)	Duration (k.y.)	Sediment supply			
				Qs, seismic (MT/yr)	Qs, total (MT/yr)	Percentage reconstructed (%)	Qs, total (km³/ Ma)
Havert	5,6*10¹⁸	2,211,880	3,800,000	1473	1795	18	711,056
Klappmyss	2,0*10¹⁸	811,885	1,400,000	1436	1701	16	776,659
Kobbe	1,7*10¹⁸	352,393	5,240,000	323	443	27	115,408
Ladinian L1	5,2*10¹⁷	287,468	4,460,000	116	169	32	24,782
Carnian C1	7,4*10¹⁷	319,985	1,700,000	434	537	19	92,378
Carnian C2	3,9*10¹⁷	293,572	1,700,000	228	280	18	72,957
Carnian C3 + 4	1,0*10¹⁸	310,610	6,300,000	160	209	23	24,495
Norian N2	1,4*10¹⁸	1,305,200	21,600,000	73	170	57	60,426

Note: Duration is based on Gilmullina et al. (2021) and Ogg et al. (2014); Havert duration is from Rossi et al. (2019).

et al., 2015; Eide et al., 2018a; Gilmullina et al., 2021), and petrographic data (Bergan and Knarud, 1993; Fleming et al., 2016). Sediment supply to the Greater Barents Sea Basin during the Triassic was much higher than in the Late Permian and varied considerably throughout the Triassic (Fig. 8). The proportion of sediments that is unconstrained by seismic data is relatively low (~25%) before the C3 + 4 interval because most of the easterly derived sediments were deposited within areas covered by seismic data (Fig. 3). For the C3 + 4 and Norian intervals, large amounts of sediment were deposited on Svalbard and in areas without seismic coverage, and the amount of reconstructed material is therefore greater.

Early Triassic

The enormous change in sediment supply from the Permian to the Triassic is particularly noteworthy (Fig. 8). Sediment supply to the Greater Barents Sea Basin increases by a factor of 25 from the Late Permian to the Early Triassic, and this high amount is sustained throughout the Early Triassic for ~5 m.y. This change represents the sudden progradation of the mudstone-dominated clinoform system (Havert and Klappmyss Formations) into the Greater Barents Sea Basin and the onset of rapid subsidence in the Early Triassic. The onset of this change is coincident with the main phase of the Siberian Traps Large Igneous Province (Burgess and Bowring, 2015), and the sustained sediment supply could indicate that significant topography and/or amounts of erodible volcaniclastic material, ash, and lava were deposited and persisted in the source area. The amount of sediment supplied to the Greater Barents Sea Basin during this time, 1850 MT/yr, is 50% greater than the sediment supply of the Amazon, which is the river with the largest drainage basin and sediment supply in the world today (Fig. 10A). In fact, the Early Triassic sediment load in the Greater Barents Sea Basin is comparable to the total sediment load of the four main rivers that drain the east side of the Andes (1640 Mt/yr; Magdalena,

Oronoco, Amazon, and Paraná), and to the entire southeast continental margin of mainland Asia (Fig. 10B) (Milliman and Farnsworth, 2013). These results indicate that during the Early Triassic, the catchment of the east sediment source had delivered amounts of sediments comparable to those of the largest active orogens in the world today despite the fact that no significant contraction was acting on the Urals Orogen at this time (Puchkov, 2009). This indicates that the Siberian Traps Large Igneous Event led to strong tectonic movement across the source area during this time. This effect is likely exacerbated by the significant global changes caused by Siberian Traps volcanism, which increased sedimentation rates across the world, on average by a factor of 7, likely due to increased global temperature and rainfall acidity that led to deforestation and increased chemical weathering (Algeo and Twitchett, 2010).

Middle Triassic

From the Early to Middle Triassic, a marked decrease in sediment load occurred. First, there was a decrease to only a quarter of the Early Triassic sediment loads into the Anisian, and then there was a further decrease to about a tenth of the Early Triassic sediment loads during the Ladinian. These sediment loads are comparable to those of some of the top 10 rivers in the world, such as the Changjiang and Orinoco Rivers for the Anisian, and the Mississippi and Mackenzie Rivers for the Ladinian (Fig. 10). Comparison with modern rivers and continental margins shows that the calculated values are reasonable and that the sediment supply from the Eastern Source became more similar to what can be expected from margins with less tectonic activity. This indicates reduced tectonic activity or increased sediment storage source area during the Middle Triassic (Fig. 10). The Kobbe Formation (Anisian) and the Ladinian stratigraphic units pinch out within the seismic data set, and there is, therefore, no potential for significant sediment bypass out of the Greater Barents Sea Basin.

Late Triassic

In the Late Triassic, a fourfold increase in sediment volume took place from the Ladinian to the Carnian C1 period. However, some sediment also prograded out of the Greater Barents Sea Basin and bypassed sediment into the seaway between Norway and Greenland (Fig. 4), and the Late Triassic sedimentation rates are therefore poorly constrained minimum estimates. This observed increase in sediment load is likely related to renewed tectonic activity in the eastern source area and possibly related to the initiation of the uplift of the Polar Urals (Puchkov, 2009). For the C2, C3 + 4, and Norian time periods, the estimated sediment volumes are relatively constant at ~250 MT/yr. These values are low compared to those of the Early Triassic and Carnian C1 time periods, but these numbers are underestimates of actual sediment transport because of significant and unconstrained sediment bypass into the seaway between Norway and Greenland for the C2 unit and also to basins to the north of the Greater Barents Sea Basin for the Carnian C3 + 4 and Norian units (Sverdrup Basin, Lomonosov High; Gilmullina et al., 2021; Fig. 2).

Modeling Results

Sediment loads modeled using the LQART-MCS approach and the parameter distributions specified in Figure 7 are presented in Figure 9 with observed and estimated sediment loads from the eastern sediment source to the Greater Barents Sea Basin (Table 2). Sediment loads from the eastern sediment source have been modeled for each of the stratigraphic units investigated, and the modeled sediment loads show broadly symmetrical bell shapes. The peaks of the bell shapes match well with the estimated sediment load of the Havert Formation (Induan), Klappmyss Formation (Olenekian), and Carnian C1, where the difference between mean modeled and estimated sediment load are 3%, 8%, and 22%, respectively. For the Kobbe Formation (Anisian), Ladinian, Carnian C2, Carnian C3 + 4, and Norian N2, the modeled sediment load is much higher (2.4×, 4.8×, 2.5×, 3.3×, and 4.0×, respectively) than the estimated sediment loads. The LQART model accounts for the suspended sediment load (Syvitski and Milliman, 2007); however, bed load is an integral part of transported sediments, which can be up to 5–6% of total sediment supply (Alexandrov et al., 2009), and represents uncertainty in our models. This uncertainty is small compared to the other uncertainties, and the low (~5%) proportion of bed load reported for other large rivers matches well with the mudstone-rich nature of the Triassic deposits of the Greater Barents Sea Basin.
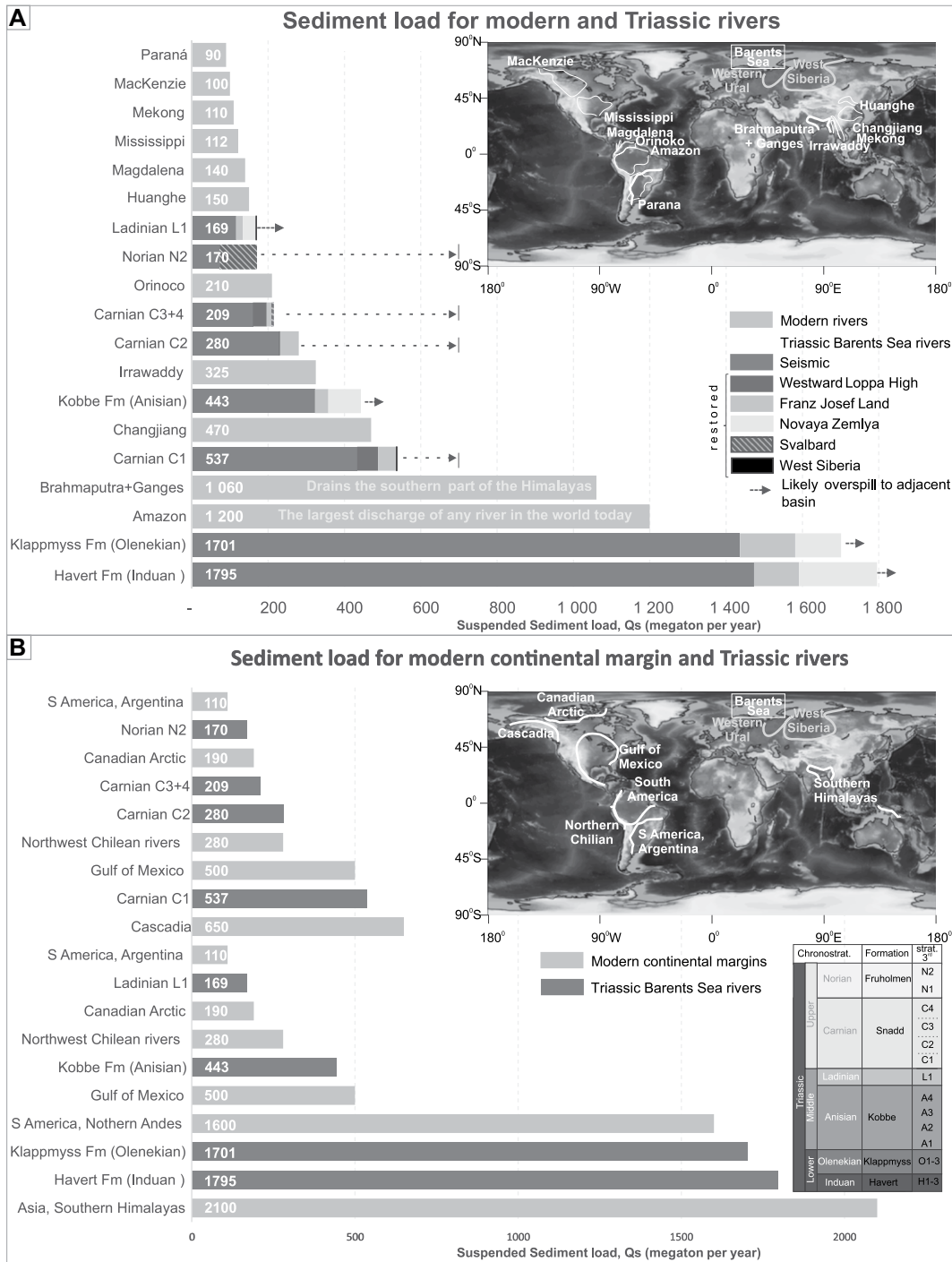
Figure 10. Comparisons show (A) sediment loads of Triassic intervals and modern river systems and (B) sediment loads of Triassic and modern continental margins.

TABLE 2. COMPARISON OF MODELLED AND MEASURED SEDIMENT LOADS (IN MT/YR) FROM THE TRIASSIC GREATER BARENTS SEA BASIN

Unit name	LQART Model			Seismic (measured ratio)
	Minimum	Mean	Maximum	
Induan	605	1603	2706	1795
Olenekian	803	1605	2912	1701
Anisian	403	1018	1928	443
Ladinian L1	268	783	1526	169
Carnian C1	129	668	1928	537
Carnian C2	162	668	1693	280
Carnian C3-4	78	668	1543	209
Norian N2	150	670	1729	170

All of the stratigraphic units older than the Carnian (Havert, Klappmyss, Kobbe, and Ladinian) show little potential for prograded over to adjacent basins because they did not prograde to the edges of the present-day Greater Barents Sea Basin. The thickness map of the Carnian C1 (Fig. 3E) unit shows that only minor amounts of sediment were bypassed outside the basin during this time interval. During the Carnian C2, Carnian C3–4, and Norian, large amounts of

sediment prograded over to adjacent basins, and the difference between the modeled sediment load and the estimated sediment load (Fig. 9) is likely explained by the amount of sediment bypassed.

For the Havert Formation, the Klappmyss Formation, and the Carnian C1, we believe that the close correspondence between modeled and estimated sediment loads means that we have a good understanding of the catchment parameters, and that little sediment was stored in sedimentary basins within the catchments. This also indicates that the BQART model has the potential to work well to investigate deep time sediment loads even in non-actualistic greenhouse settings. These stratigraphic units show only minor sediment bypass to adjacent sedimentary basins.

The Kobbe Formation (Anisian) and the Ladinian stratigraphic unit are constrained within the seismic data set and have little potential for sediment bypass to adjacent basins (Fig. 3), but they still show a significant mismatch between the modeled and estimated sediment load values. The most uncertain variable in the LQART modeling is the relief, and even if the relief is changed to low values (max relief is 0.5–1.5 km across the entire catchment) in the modeling, the modeled sediment loads are still much higher than the estimated sediment loads. This suggests that significant sediment storage must have taken place within the catchment of the eastern sediment source during the Early Triassic.

Grain-size trends observed in the most proximal eastern parts of the Greater Barents Sea Basin (Gilmullina et al., 2021) are consistent with the modeling results above: the Lower Triassic formations in the Timan-Pechora Basin contain large amounts of conglomerates (Morakhovskaja, 2000), which suggests that these were deposited close to the sediment source. In the Middle and Late Triassic, the grain-size in this proximal basin decreased to fine-medium grain size (Morakhovskaja, 2000), which indicates that more proximal sedimentary basins started subsiding and extracted coarser sediment. This implies that currently unknown or now eroded Middle Triassic deposits should have been deposited in the Volga-Urals Basin and in West Siberia. Biostratigraphic and thermochronological data from these basins should be investigated to see if there is evidence for burial at this time.

Contributors to Variability in Sediment Load Models

How the different parameters in the LQART models contribute to variance in the modeled sediment load is shown in Figure 9. For most of the stratigraphic units, the variability is mostly explained by temperature followed by lithology. This means that even within the large bounds we

have set for relief and catchment area (Fig. 7), the main variability is caused by parameters that are very difficult to account for. For the Early Triassic units, the great uncertainty in the height of the Urals is carried into the modeling result, but the modeling results still show significant differences from the younger stratigraphic units.

Urals as the Only Sediment Source of the Greater Barents Sea Basin?

The Ural Mountain range has traditionally been considered the only source of the Triassic sediments of the Barents Sea (e.g., Bergan and Knarud, 1993; Flowerdew et al., 2019). The tectonic evolution of the Novaya Zemlya Fold and Thrust Belt remained enigmatic and was considered to be a barrier to sediment supplied from the West Siberian Basin to the Greater Barents Sea Basin. However, clinoform geometries from the Induan (fig. 41 in Norina et al., 2014), constant thickness trends toward the Novaya Zemlya Fold and Thrust belt throughout the Lower Triassic (Gilmullina et al., 2021), and evidence for extensive sedimentary recycling in the Greater Barents Sea Basin in the Late Triassic and Jurassic (Zhang et al., 2018b; Haile et al., 2021) all indicate that uplift of the Novaya Zemlya Fold and Thrust Belt occurred in the Late Triassic (Fig. 5). Here, we investigate if the estimated sediment loads are consistent with a sediment source from the Western Urals Catchment only (Fig. 3), or if the sediment loads and models require a larger catchment. This would imply that the early uplift (Carnian–Norian) of Novaya Zemlya did not create topography high enough to serve as a barrier to sediment supply from West Siberia and the Greater Barents Sea Basin.

LQART-MCS modeling using only an enclosed area between the Urals and Fennoscandia as a sediment source requires unrealistic catchment parameter values to deliver the observed sediment loads. The required relief in the Western Urals Catchment is 12 ± 2 km for the Early Triassic and 10 ± 1 km for the Carnian C1 unit. These relief values are clearly unrealistic as they are higher than 9 km, which is higher than the maximum possible height of mountain ranges on Earth (e.g., Molnar and Lyon-Caen, 1988). The established size of the Western Urals Catchment is based on published material described above, and there is no realistic expansion of the catchment further westward. For the same catchment area not including the Western Urals source, an increase of temperature will require an increase up to an average of 45 ± 1.7 °C in the Permian-Triassic boundary and from 12 ± 1.3 °C in the Middle Triassic to 25 ± 1.7 °C in the Late Triassic, which is also unrealistic (Sun et al., 2012; Scotese and Moore, 2014). To explain this increase with a change in the lithology factor, the

entire catchment would have to be dominated by loess, which contradicts the geological evolution of the catchment area that includes the Urals, Fennoscandia, and the Voronezh high. Thus, according to the LQART-MCS-model, the estimated sediment loads are too high to be supplied by the Western Urals Catchment alone and require that the West Siberian Catchment also contributed as a catchment to the Greater Barents Sea Basin in the Triassic. This conclusion is supported by detrital zircons from the Eastern Barents Sea wells (Khudoley et al., 2019), and Franz Josef Land (Soloviev et al., 2015), which indicates that the West Siberian basement is one of the sources of the Triassic sediments.

DISCUSSION

The Triassic sedimentary system in the Greater Barents Sea Basin developed over 50 m.y. during which there were major tectonic events and climate changes. In the following sections, we discuss catchment extent, how estimated and modeled sediment supply fit together, and which events could have affected the sedimentary system. Then we compare the Triassic Greater Barents Sea Basin system with other big, ancient systems.

Catchment Extent

Clinoform (Glørstad-Clark et al., 2010) and channel (Klausen et al., 2015) directions combined with sediment budget calculations and BQART modeling of the sediment supply in this study give clues to the extent and geological evolution of the catchment area. The Central Asian Orogenic Belt, with the West Siberian Basin, was an important source of clastic material (Khudoley et al., 2019). The West Siberian Basin contains interbedded clastic material and volcanoclastics and likely served as both a pathway for sediment from the Central Asian Orogenic Belt and as a sediment source from uplifted rift shoulders (Vyssotski et al., 2006; Meshcheryakov and Karaseva, 2010) or valley interfluves (Sømme et al., 2018). The Siberian Traps Large Igneous Province was probably less a contributor to the Greater Barents Sea Basin due to the low erodibility of basalt lavas, and relatively good preservation today, and lack of chrome-spinels with a clear large igneous province signature in the Greater Barents Sea Basin at least in the Carnian (Harstad et al., 2020). The role of the Taimyr source was discussed in many publications and accounted for in the modeling here, but the small size and position away from main sediment fairways measured from clinoforms and channel directions indicates that Taimyr was only one of many sources and that it

would be difficult for large amounts of sediment from Taimyr to reach the areas studied in Svalbard. Even though the Western Urals Catchment included a large territory from Fennoscandia to the Urals, the estimated sediment volumes (Fig. 8) require a much larger catchment that includes West Siberia and the Central Asian Orogenic Belt according to the LQART models.

The exact distribution and thickness of the Middle and Late Triassic deposits in the catchment area remain unknown and require further investigation by thermochronologic data and basin modeling. Detrital thermochronology of the Greater Barents Sea Basin during the Triassic using methods with different closure temperatures would be extremely useful in constraining sediment sources and source area evolution and could help determine the relative magnitude of sediment sources from areas with protracted (e.g., Central Asian Orogenic Belt) or sudden (Siberian Traps) volcanic activity or mainly basin inversion/sediment recycling.

Comparison of Modeled and Observed Sediment Load

Observed and modeled sediment load show an excellent match in some of the time units (Lower Triassic and Carnian C1). In the Middle Triassic and the stratigraphic units younger than Carnian 1 (Carnian C2, Carnian C3 + 4, and Norian N2; Fig. 2), the observed sediment loads are lower than what is predicted by the models. Here we discuss plausible interpretations of this.

Lower Triassic

The Lower Triassic is well-mapped and almost fully constrained within the seismic data in the Greater Barents Sea Basin. The Havert and Klappmyss units have high estimated sediment loads, which lie within 8% of the mode of the sediment loads modeled using LQART-Monte Carlo simulations (Fig. 9). Only minor amounts of sediment bypass might have occurred in the North Kara Sea toward the Lomonosov Ridge, as the rest of the Lower Triassic sedimentary units are contained within the seismic data (Figs. 3 and 6). Comparison of the results to the modeled sediment loads with the expected catchment properties confirms that the LQART-Monte-Carlo simulations give reasonable results and shows that the Lower Triassic system in the Barents Sea must have been able to supply an exceptionally high sediment load due to high mountains (or high tectonic activity), warm catchment temperature, and a huge catchment.

Middle Triassic

The Anisian unit is mapped in the seismic data and fully constrained within the seismic data except for the North Kara Sea, where some bypass toward the Lomonosov Ridge would have occurred, similar to bypass at the Induan and Olenekian units (Fig. 3). The estimated sediment is ~40% of the mode of the modeled sediment loads and plots just above the minimum value of the modeled sediment load.

The Ladinian L1 unit is mapped within the Greater Barents Sea Basin and shows progradation toward the North Kara Sea, where some bypass toward the Lomonosov Ridge would have occurred, and toward the North Atlantic margin, where the deposits are heavily faulted and buried too deeply to be confidently interpreted. The estimated sediment load for the Ladinian L1 is less than the minimum modeled value and only 20% of the mode of the modeled sediment volumes.

One possible explanation for the low estimated sediment loads in the Middle Triassic could be bypass toward the north for the Anisian and also toward the west for the Ladinian L1. However, the limited progradation of the Middle Triassic units toward the northwest compared to the Early and Late Triassic makes this unlikely to be the case. Another possible explanation could be that the expected values for the Middle Triassic are too high, but even model runs with input values that are unrealistically low (i.e., catchment relief between 0.5 km and 1 km, catchment area is 50% of preferred catchment, catchment temperature is 2 °C lower than likely temperature) cannot recreate the low estimated sediment loads. Our preferred explanation for the low estimated sediment loads in the Middle Triassic is, therefore, that the sediment that otherwise would have been supplied to the Greater Barents Sea Basin was stored in the catchment area and later was eroded by post-Triassic events in the East European Platform or buried underneath the thick Jurassic–Paleogene succession in the West Siberian Basin. This would imply rapid subsidence in the Western Urals and West Siberian Catchment areas during the Middle Triassic and could perhaps be a response to crustal cooling after the Siberian Traps Large Igneous Province.

Late Triassic

Late Triassic units are only partially mapped within the Greater Barents Sea Basin. Reasons for that are the Upper Triassic strata (1) prograded beyond the Greater Barents Sea Basin into the western margin, where they are strongly faulted and buried below thick Cretaceous to recent deposits; and (2) prograded into the areas that are now exposed on Svalbard and beyond the Greater Barents Sea Basin toward the northwest and north (Fig. 3), and locally the strata were eroded by the Triassic–Jurassic unconformity, the base Cretaceous uncon-

formity, and the upper regional unconformity (Figs. 2–3). The Carnian C1 unit is the last unit mapped within the Greater Barents Sea Basin that was constrained well-enough that sediment volumes could be restored with some degree of confidence. For the younger Carnian and Norian units, the estimated sediment loads are minimum estimates, and significant sediment bypass must have affected adjacent basins.

The Carnian C1 unit has a high estimated sediment load that lies within 78% of the mode of the modeled range. The estimated volume of the younger Late Triassic units (C2, C3 + 4, and N2) is toward the lower end of the modeled sediment load range and constitutes 40%, 30%, and 25% of the mode of the modeled sediment loads, respectively.

The comparison of the modeled and estimated sediment load for the Carnian C1 unit again shows a good fit and favors the chosen model parameters. There is no reason to believe that catchment properties in the intra-Carnian and Norian units were dramatically different than in the preceding time units because the petrographic and detrital zircon age data are similar (Omma, 2009; Bue and Andresen, 2013; Fleming et al., 2016; Klausen et al., 2017; Flowerdew et al., 2019). Thus, a large mismatch between modeled and estimated sediment load for the C2, C3 + 4, and N2 units suggests a loss of a significant amount of sediment from the Greater Barents Sea Basin. The most probable explanation for this underbalanced sediment budget is that the sediment supplied to the Greater Barents Sea Basin in the Late Triassic prograded over to the adjacent Arctic basins, such as the Sverdrup Basin, which at the time were located much closer to the Barents Sea (Figs. 4–5; Shephard et al., 2014). Sediment transport directions in the Triassic Greater Barents Sea Basin show a continuous NW progradation, and the breakup of the North Barents Sea margin in the Paleogene and the NW Atlantic in the Eocene appears to have separated the Greater Barents Sea Basin from the more distal locations. Analysis of detrital zircon data from the Carnian and Norian sediments of the Sverdrup Basin (Miller et al., 2006; Omma et al., 2011; Anfinson et al., 2016) show a detrital zircon age signature very similar to what is seen in the sediments from the Eastern Source (Urals and West Siberia) of the Greater Barents Sea Basin. This strongly indicates sediment transport through the Greater Barents Sea Basin to the Sverdrup Basin in the Late Triassic.

Response of the Triassic System to Large-Scale Climatic and Tectonic Perturbations

The Permian-Triassic boundary marks a catastrophic event caused by the largest volcanic

eruption in the Earth's history, which is believed to be one of the reasons that led to extreme warming and mass extinction in the Early Triassic (Reichow et al., 2009; Sun et al., 2012). The prime cause of the chain of events is debated but might have been caused by the amalgamation of a large continental landmass that led to an accumulation of internal heat, surface uplift, and the development of a Large Igneous Province (Peace et al., 2020). The concentration of magma beneath East Siberia likely caused uplift, which resulted in an unconformity in the distal parts of the Siberian Traps in the Timan-Pechora Basin prior to the eruption (Prischepa et al., 2011). More proximal to the Siberian Traps, the West Siberian Basin appears to have a graben and basin topography where sedimentation tends to be a mix of Siberian Traps basalts and coarse-grained clastic material (Meshcheryakov and Karaseva, 2010; Fig. 4). The onset of volcanism appears to have led to the reactivation of proximal adjoining orogens such as the Urals (Puchkov, 2009), great sediment supply, and strong subsidence in more distal basins as the Greater Barents Sea Basin (Glørstad-Clark et al., 2010; Gilmullina et al., 2021). A widespread unconformity developed over the Timan-Pechora Basin (Prischepa et al., 2011), Fennoscandia (Eide et al., 2018a), Greenland and Svalbard (Sørkapp-Hornsund High) (Zuchuat, 2014; Bjerager et al., 2019), and North Kara terrane (Drachev, 2016), and voluminous siliciclastic sedimentation created exceptional conditions, which resulted in higher sedimentation rates in the Lower Triassic in the Greater Barents Sea Basin. Despite a semi-arid climate, high sedimentation rates were compensated by a large amount of upland that was exposed in the Early Triassic.

In addition, the consequences of the Siberian Trap eruption increased the acidity of precipitation, which led to increased chemical weathering. This, combined with a rapidly warming climate, likely led to the destruction of terrestrial vegetation and increased soil erosion, which led to increased sediment runoff (Algeo and Twitchett, 2010) that resulted in high sediment supply and large-scale progradation of the Lower Triassic wedges (Gilmullina et al., 2021). The effects of climatic changes and increased weathering were shown by Algeo and Twitchett (2010) to have led to an increase in sedimentation by a factor of seven from the Late Permian to the Early Triassic. However, the sediment supply rates in the Greater Barents Sea Basin increased by a factor of ~150 across the Permian–Triassic boundary (Fig. 8), which strongly suggests that this increase was forced mainly by tectonics and not by climate and Siberian Trap emplacement.

The main phase of activity of the Siberian Traps in the catchment area concluded in the Early Triassic (Reichow et al., 2009), which is expressed in the low sedimentation rates in the Greater Barents Sea Basin in the Middle Triassic (Fig. 8). The Middle Triassic was also characterized by a high global sea-level rise which, with a combination of relatively low sedimentation rates, led to deposition of the source rock of the Steinkobbe Formation in the Greater Barents Sea Basin.

In the Greater Barents Sea Basin, the Upper Triassic sediment load increased again after relatively low sedimentation rates in the Ladinian period. This increase coincides with a change in the main depocenter location from east to west in Greater Barents Sea Basin.

After the Early Triassic, the relatively arid global greenhouse climate started to change, and by the Late Triassic, the study area was characterized by a humid and warm climate, which facilitated the deposition of ubiquitous coal beds. A worldwide humid episode known as the Carnian Pluvial Event (Simms and Ruffell, 1989; Mueller et al., 2016; Ruffell et al., 2016), which is linked to the Wrangelian Large Igneous Province eruption in Alaska, likely triggered climatic change and increased runoff of siliciclastic sediments (Dal Corso et al., 2018). High precipitation combined with increased tectonic activity could have resulted in a new relatively high peak in sediment supply in the Carnian and sediment supply from upland regions, where rainfall was otherwise more subdued.

Comparing Late Permian and Triassic Sediment Transport

It has been inferred that during the Late Permian, before emplacement of the Siberian Traps Large Igneous Province, the paleo-Lena and the paleo-Khatanga Rivers drained the Eastern Urals, West Siberia, and the Central Asian Orogenic Belt and transported this sediment northward to the Arctic (Miller et al., 2013; Ershova et al., 2016). Sediments from the W Urals were transported by the Paleo-Ural River (Miller et al., 2013; Ershova et al., 2016) and confined to the W Uralian foreland basin and the SE extremes of the Greater Barents Sea Basin, while the W Greater Barents Sea Basin was mainly a site of carbonate and spiculite deposition (e.g., Worsley et al., 2008). Based on the results presented herein, we show that this setting changed after the Permian–Triassic transition, and sediment from the Central Asian Orogenic Belt and West Siberia was then routed into the Greater Barents Sea Basin and from there to basins beyond (Fig. 4). There are probably three main reasons why the sediment routing changed in this way at the onset of the Triassic.

Firstly, during the Permian, ongoing contraction in the Urals created subsidence rates in the W Urals foreland basin that were so high that sediment could not fill that basin and prograde out into the Greater Barents Sea Basin. As contraction rates decreased during the Late Permian (Puchkov, 2009), subsidence and the potential for sediment storage here decreased. Later sediment pulses in the Triassic could therefore reach the Greater Barents Sea Basin. Secondly, Early Permian reconstructions show orogenic terrain in the Northern Urals and southern Kara Sea (Vernikovsky et al., 2020). This terrain probably deflected sediment routing systems from West Siberia and the Central Asian Orogenic Belt away from the Greater Barents Sea Basin and toward the northern Arctic margin. Rifting in West Siberia in the Late Permian (Nikishin et al., 2002) likely created a pathway that facilitated sediment transport toward the NW. Finally, tectonic reorganization, widespread volcanism, and regional uplift associated with the Siberian Traps Large Igneous Province led to abundant sediment supply in the Early Triassic that reached the Greater Barents Sea Basin facilitated by slow subsidence in the Western Urals foreland basin and by a rift topography in West Siberia and the South Kara Sea (Fig. 5).

Comparison of Ancient and Modern Systems

Selected case studies of well-known large fluvial systems were used to put the results from the Greater Barents Sea Basin in context and to better understand the Triassic sedimentary system in light of modern analogues with known constraints on catchment configuration.

The sediment flux of the paleo-Orange River in southern Africa, which drains the Southern African Plateau, varied dramatically during the Cretaceous and Cenozoic (Fig. 11). Braun et al. (2014) link the extreme increase in sedimentation rates in the Late Cretaceous with the migration of the African continent over a mantle plume that caused major plateau uplift. The sedimentation rate increased ninefold at the beginning of the Turonian, when the area approached the plume, and decreased fourteenfold at the end of the Maastrichtian, when the area passed the plume. This trend is similar to that observed in the Greater Barents Sea Basin during the Early Triassic; there is a sudden increase of sediment supply at the Permian–Triassic boundary and a decrease in the Lower–Middle Triassic (Fig. 8). However, the magnitude of the changes in the Triassic Greater Barents Sea Basin is much larger; there is a ~25× increase versus a factor of 9 for the Orange River example. This may be because the Siberian Traps Large Igneous
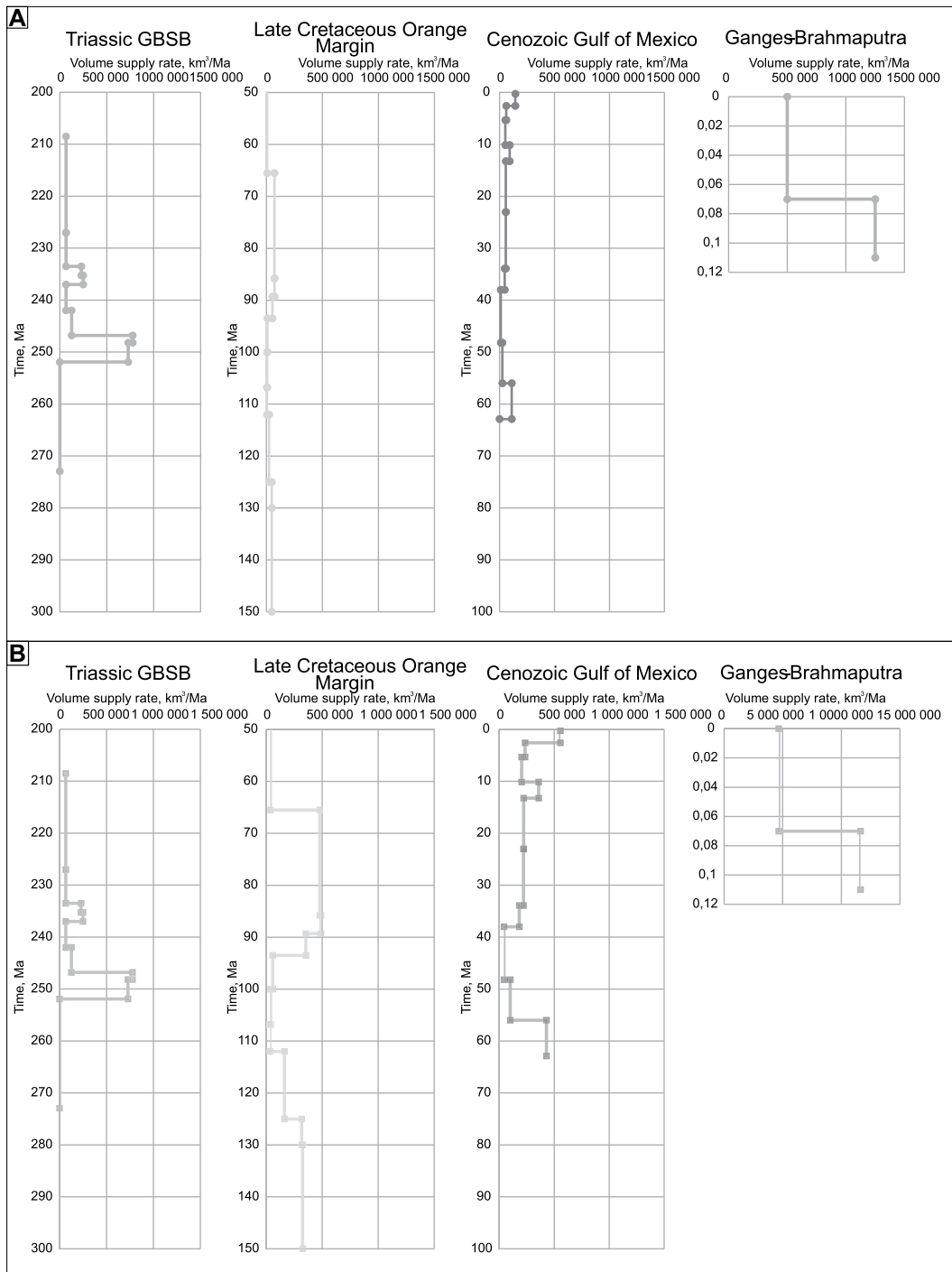
Figure 11. Comparisons show sediment loads of the Triassic intervals and ancient river system of the Orange River margin and Gulf of Mexico and Ganges and Brahmaputra River system over the last 11,000 yr. (A) Original sediment volume supply rate for modern and Triassic rivers (Braun et al., 2014; Galloway et al., 2011; Goodbred and Kuehl, 2000); (B) sediment load for modern continental margin and Triassic rivers. Sediment supply is normalized by the size of the Greater Barents Sea Basin Triassic Catchment area (normalized sediment supply rate = (sediment supply rate * (Triassic Greater Barents Sea Basin Catchment/modern catchment)).

Province was much larger than the South African Large Igneous Province and was associated with much greater climatic effects (Algeo and Twitchett, 2010). The duration of exposure to large igneous province activity also was much shorter for the Greater Barents Sea Basin (4.7 m.y. vs. 25 m.y.) (Fig. 11).

The Gulf of Mexico is a well-studied area where the sedimentation rate was very high and comparable to that of the Orange River margin

(Fig. 11). An increase in sedimentation rates in the late Paleocene–middle Eocene (Wilcox Formation) was linked by Galloway et al. (2011) primarily to tectonic and climate factors. The Orange River margin and Gulf of Mexico systems both responded to changing tectonic settings at the same order of magnitude as the Middle and Late Triassic. Furthermore, the Middle and Late Triassic were characterized by moderate tectonic settings.

Goodbred and Kuehl (2000) suggested that a dramatic change in the Ganges-Brahmaputra sediment discharge was a response to climatic change. The southwestern monsoon brought warm and humid air to the Himalayan Range that increased precipitation, runoff, and discharge (Fig. 11). The Lower Triassic in the Greater Barents Sea Basin and the Ganges-Brahmaputra are similar systems, with extreme sedimentation rates and tectonic activity in the catchment

area; however, the nature of climatic change is different in these two areas. Extreme values in the Greater Barents Sea Basin Lower Triassic are probably linked to a larger magmatic field and major uplift, acidic precipitation, and the resultant low vegetation cover. Thus, increased precipitation caused by the monsoon is more similar to the effects of the Carnian Pluvial Event of the Late Triassic, which was probably responsible for the increase in sediment load in the Carnian C1 unit. Despite extreme climatic and tectonic events, the LQART modeling covers the estimated sediment load, and though the model was calculated for modern rivers, it seems to work for ancient systems as well.

One of the greatest problems for understanding the Triassic system in the Greater Barents Sea Basin and how it changed through time is the lack of appropriate modern analogues. None of the largest modern river drainage systems are directly related to hotspots or large igneous provinces.

The response of the Triassic system from source-to-sink, which reflects climatic and tectonic changes in the Early and Late Triassic, led to a dramatic increase in sediment discharge. In some ways, modern climatic changes and human activity such as deforestation could be similar to conditions in the past, and it is possible that the Triassic could be a useful example for understanding extreme transformations in Earth history. Nevertheless, there are some challenges to overcome before a direct comparison can be made. Firstly, the low age resolution in deep time systems makes it difficult to compare records of such systems to those of recent systems. Secondly, in the Triassic it is difficult to know the relative contribution of important factors such as climate and tectonic activity. With more precise thermochronological data, it could be easier to deconvolve these two factors.

CONCLUSION

This study explored changes in the rates of sediment supplied to the Greater Barents Sea Basin throughout the Triassic by investigating large amounts of seismic reflection and well data. The calculated sediment load values were corrected for erosion and related to catchment properties by using Monte Carlo simulations of the LQART sediment supply model. Our results show that:

(1) Estimated and modeled sediment loads of the Lower Triassic are very similar, extremely high, and match those of the biggest modern river systems with sources in the most tectonically active orogens (Himalayas and Andes) today;

(2) The Middle Triassic sediment load was significantly lower but still comparable to that of the top 10 biggest modern rivers, and ancient counterparts (Paleogene Wilcox Formation, Gulf of Mexico). In addition, seismic and modeled sediment loads show a significant mismatch, which likely indicates storage of sediment in the catchment area and/or low tectonic activity;

(3) Another high peak in sediment supply occurred in the Late Triassic and coincided with a westward depocenter shift in the Greater Barents Sea Basin. The Upper Triassic contains four time units, three of which show a considerable mismatch between observed and modeled sediment load, which we link strongly with significant sediment bypass to adjacent basins in the Carnian and Norian.

We suggest that the Early Triassic sediment supply was a direct and indirect result of emplacement of the Siberian Traps Large Igneous Province, which caused reactivation and uplift of adjacent orogens and global climatic change that led to increased weathering and possibly the collapse of vegetation. The sediment supply was so large that it could only be explained by the Greater Barents Sea Basin being supplied from catchments on both sides of the Urals, which indicates that the Greater Barents Sea Basin was sourced from both the Western Urals foreland basin and West Siberia and likely included the eastern parts of the Urals, parts of the Siberian Traps, and the Central Asian Orogenic Belt. This large amount of sediment caused great subsidence in the Eastern Barents Sea.

The Middle Triassic sediment supply possibly shows a relaxation of topography and subsidence in the source area after intensive volcanism. This lowered sediment supply led to the widespread extent of the source rock of the Steinkobbe Formation in the Greater Barents Sea Basin.

The Upper Triassic sediment supply increased after relatively low supply during the Ladinian and coincided with the Carnian Pluvial Event and the last reactivation of the Northern Urals, which is likely a primary reason for high sediment delivery to the Greater Barents Sea Basin. The Late Carnian and Norian stratigraphic intervals show sedimentary evidence of bypass to adjacent sedimentary basins toward the W, NW, and W, and the estimated sediment volumes of these time units are smaller than what the LQART model would predict. This implies the bypass of large amounts of sediment from the Urals and West Siberian sediment source into the adjacent Lomonosov Ridge, Sverdrup Basin, and Chukotka in the Late Carnian and Norian.

ACKNOWLEDGMENTS

REFERENCES CITED

Alexandrov, Y., Cohen, H., Laronne, J.B., and Reid, I., 2009, Suspended sediment load, bed load, and dissolved load yields from a semiarid drainage basin: A 15-year study: Water Resources Research, v. 45, no. 8, https://doi.org/10.1029/2008WR007314.

Algeo, T.J., and Twitchett, R.J., 2010, Anomalous Early Triassic sediment fluxes due to elevated weathering rates and their biological consequences: Geology, v. 38, no. 11, p. 1023–1026, https://doi.org/10.1130/G31203.1.

Anfinson, O.A., Embry, A.F., and Stockli, D.F., 2016, Geochronologic constraints on the Permian–Triassic northern source region of the Sverdrup Basin, Canadian Arctic Islands: Tectonophysics, v. 691, p. 206–219, https://doi.org/10.1016/j.tecto.2016.02.041.

Augland, L.E., Ryabov, V.V., Vernikovsky, V.A., Planke, S., Polozov, A.G., Callegaro, S., Jerram, D.A., and Svensen, H.H., 2019, The main pulse of the Siberian Traps expanded in size and composition: Scientific Reports, v. 9, no. 1, article no. 18723, https://doi.org/10.1038/s41598-019-54023-2.

Bergan, M., and Knarud, R., 1993, Apparent changes in clastic mineralogy of the Triassic–Jurassic succession, Norwegian Barents Sea: Possible implications for palaeodrainage and subsidence, in Vorren, T.O., Bergsager, E., Dahl-Stamnes, Ø.A., Holter, E., Johansen, B., Lie, E., and Lund, T.B., eds., Norwegian Petroleum Society Special Publication, Volume 2: Amsterdam, Elsevier, p. 481–493, https://doi.org/10.1016/B978-0-444-88943-0.50034-4.

Bjerager, M., Alsen, P., Hovikoski, J., Lindström, S., Pilgaard, A.S., Stemmerik, L., and Therkelsen, J., 2019, Triassic lithostratigraphy of the Wandel Sea Basin, North Greenland: Bulletin of the Geological Society of Denmark, v. 67, no. 1, https://doi.org/10.37570/bgsd-2019-67-06.

Braun, J., Guillocheau, F., Robin, C., Guillaume, B., and Jelsma, H., 2014, Rapid erosion of the Southern African Plateau as it climbs over a mantle superswell: Journal of Geophysical Research: Solid Earth, v. 119, no. 7, p. 6093–6112, https://doi.org/10.1002/2014JB010998.

Bue, E.P., and Andresen, A., 2014, Constraining depositional models in the Barents Sea region using detrital zircon U–Pb data from Mesozoic sediments in Svalbard, in Scott, R.A., Smyth, H.R., Morton, A.C., and Richardson, N., Sediment Provenance Studies in Hydrocarbon Exploration and Production: Geological Society, London, Special Publication 386, no. 1, p. 261–279, https://doi.org/10.1144/SP386.14.

Bukina, T.F., and Yanochkina, Z.A., 2011, Triassic Beds from the Pricaspian Depression (Lithology-Stratigraphy Study) [in Russian]: Izvestiya of Saratov University: v. 11, no. 1, p. 51–57.

Burgess, S.D., and Bowring, S.A., 2015, High-precision geochronology confirms voluminous magmatism before, during, and after Earth's most severe extinction: Science Advances, v. 1, no. 7, p. e1500470, https://doi.org/10.1126/sciadv.1500470.

Chumakov, N., and Zharkov, M., 2003, Climate during the Permian–Triassic biosphere reorganizations. Article 2. Climate of the Late Permian and Early Triassic:

General inferences: Stratigraphy and Geological Correlation, v. 11, no. 4, p. 361–375.

Crameri, F., 2018, Geodynamic diagnostics, scientific visualisation and StagLab 3.0: Geoscientific Model Development, v. 11, p. 2541–2562, https://doi.org/10.5194/gmd-11-2541-2018.

Dal Corso, J., et al., 2018, Multiple negative carbon-isotope excursions during the Carnian Pluvial Episode (Late Triassic): Earth-Science Reviews, v. 185, p. 732–750, https://doi.org/10.1016/j.earscirev.2018.07.004.

Daragan-Sushchova, L., Petrov, O., Daragan-Sushchov, Y.I., and Vasil'ev, M.A., 2014, Structure of the North Kara Shelf from results of seismostratigraphic analysis: Geotectonics, v. 48, no. 2, p. 139–150, https://doi.org/10.1134/S0016852114020022.

Doré, A., Lundin, E., Gibbons, A., Sømme, T.O., and Tørudbakken, B.O., 2016, Transform margins of the Arctic: A synthesis and re-evaluation, in Nemčok, M., Rybár, S., Sinha, S.T., Hermeston, S.A., and Ledvényiová, L., eds., Transform Margins: Development, Controls and Petroleum Systems: Geological Society, London, Special Publication 431, no. 1, p. 63–94, https://doi.org/10.1144/SP431.8.

Døssing, A., Gaina, C., Jackson, H.R., and Baltazar Andersend, O., 2020, Cretaceous ocean formation in the High Arctic: Earth and Planetary Science Letters, v. 551, no. 116552, https://doi.org/10.1016/j.epsl.2020.116552.

Drachev, S.S., 2016, Fold belts and sedimentary basins of the Eurasian Arctic: Arktos, v. 2, no. 21, http://dx.doi.org/10.1007/s41063-015-0014-8.

Dypvik, H., Sokolov, A., Pcelina, T., Dypvik, H., Sokolov, A., Pcelina, T., Fjellsa, B., Bj.rke, T., Korchinskaya, M., and Nagy, J., 1998, The Triassic successions of Franz Josef Land, stratigraphy and sedimentology of three wells from Alexandra, Hayes and Graham-Bell islands. Geological aspects of Franz Josef Land and the northernmost Barents Sea—the Northern Barents Sea Geotraverse: Norsk Polarinstitutt Meddelelser, v. 151, p. 50–82.

Eide, C.H., Schofield, N., Jerram, D.A., and Howell, J.A., 2017, Basin-scale architecture of deeply emplaced sill complexes: Jameson Land, East Greenland: Journal of the Geological Society, v. 174, no. 1, p. 23–40, https://doi.org/10.1144/jgs2016-018.

Eide, C.H., Klausen, T.G., Katkov, D., Suslova, A.A., and Helland-Hansen, W., 2018a, Linking an Early Triassic delta to antecedent topography: Source-to-sink study of the southwestern Barents Sea margin: Geological Society of America Bulletin, v. 130, no. 1–2, p. 263–283, https://doi.org/10.1130/B31639.1.

Eide, C.H., Müller, R., and Helland-Hansen, W., 2018b, Using climate to relate water discharge and area in modern and ancient catchments: Sedimentology, v. 65, no. 4, p. 1378–1389, https://doi.org/10.1111/sed.12426.

Embry, A., 1993, Crockerland—the northwest source area for the Sverdrup Basin, Canadian Arctic Islands, in Vorren, T.O., Bergsager, E., Dahl-Stamnes, Ø.A., Holter, E., Johansen, B., Lie, E., and Lund, T.B., eds., Norwegian Petroleum Society Special Publication, Volume 2: Amsterdam, Elsevier, p. 205–216, https://doi.org/10.1016/B978-0-444-88943-0.50018-6.

Embry, A., 2011, Petroleum prospectivity of the Triassic–Jurassic succession of Sverdrup Basin, Canadian Arctic Archipelago, in Spencer, A.M., Embry, A.F., Gautier, D.L., Stoupakova, A.V., and Sørensen, K., eds., Arctic Petroleum Geology: Geological Society, London, Memoir 35, p. 545–558, https://doi.org/10.1144/M35.36.

Ershova, V.B., Prokopiev, A.V., Khudoley, A.K., Sobolev, N.N., and Petrov, E.O., 2015, U/Pb dating of detrital zircons from late Palaeozoic deposits of Bel'kovsky Island (New Siberian Islands): Critical testing of Arctic tectonic models: International Geology Review, v. 57, no. 2, p. 199–210, https://doi.org/10.1080/00206814.2014.999358.

Ershova, V.B., et al., 2016, Trans-Siberian Permian rivers: A key to understanding Arctic sedimentary provenance: Tectonophysics, v. 691, p. 220–233, https://doi.org/10.1016/j.tecto.2016.03.028.

Fleming, E.J., Flowerdew, M.J., Smyth, H.R., Scotta, R.A., Morton, A.C., Omma, J.E., Frei, D., and Whitehouse, M.J., 2016, Provenance of Triassic sandstones on the southwest Barents Shelf and the implication for sediment dispersal patterns in northwest Pangaea: Marine and Petroleum Geology, v. 78, p. 516–535, https://doi.org/10.1016/j.marpetgeo.2016.10.005.

Flowerdew, M.J., Fleming, E.J., Morton, A.C., Frei, D., Chew, D.M., and Daly, J., 2019, Assessing mineral fertility and bias in sedimentary provenance studies: Examples from the Barents Shelf, in Downey, P.J., Osborne, M., and Volk, H., eds., Geological Society, London, Special Publication 484, p. 255–274, https://doi.org/10.1144/SP484.11.

Gac, S., Huismans, R.S., Podladchikov, Y.Y., and Faleide, J.I., 2012, On the origin of the ultradeep East Barents Sea basin: Journal of Geophysical Research: Solid Earth, v. 117, no. B4, https://doi.org/10.1029/2011JB008533.

Gac, S., Klitzke, P., Minakov, A., Faleide, J.I., and Scheck-Wenderoth, M., 2016, Lithospheric strength and elastic thickness of the Barents Sea and Kara Sea region: Tectonophysics, v. 691, p. 120–132, https://doi.org/10.1016/j.tecto.2016.04.028.

Galloway, W.E., Whiteaker, T.L., and Ganey-Curry, P., 2011, History of Cenozoic North American drainage basin evolution, sediment yield, and accumulation in the Gulf of Mexico basin: Geosphere, v. 7, no. 4, p. 938–973, https://doi.org/10.1130/GES00647.1.

Gilmullina, A., Klausen, T.G., Paterson, N.W., Suslova, A., and Haug Eide, C., 2021, Regional correlation and seismic stratigraphy of Triassic strata in the Greater Barents Sea: Implications for sediment transport in Arctic basins: Basin Research, v. 33, p. 1546–1579, https://doi.org/10.1111/bre.12526.

Glørstad-Clark, E., Faleide, J.I., Lundschien, B.A., and Nystuen, J.P., 2010, Triassic seismic sequence stratigraphy and paleogeography of the western Barents Sea area: Marine and Petroleum Geology, v. 27, no. 7, p. 1448–1475, https://doi.org/10.1016/j.marpetgeo.2010.02.008.

Goodbred, S.L., Jr., and Kuehl, S.A., 2000, Enormous Ganges-Brahmaputra sediment discharge during strengthened early Holocene monsoon: Geology, v. 28, no. 12, p. 1083–1086, https://doi.org/10.1130/0091-7613(2000)28<1083:EGSDDS>2.0.CO;2.

Grasby, S.E., Knies, J., Beauchamp, B., Bond, D.P.G., Wignall, P., and Sun, Y., 2020, Global warming leads to Early Triassic nutrient stress across northern Pangea: Geological Society of America Bulletin, v. 132, no. 5–6, p. 943–954, https://doi.org/10.1130/B32036.1.

Hadlari, T., Dewing, K., Matthews, W.A., Alonso-Torres, D., and Midwinter, D., 2018, Early Triassic development of a foreland basin in the Canadian high Arctic: Implications for a Pangean Rim of Fire: Tectonophysics, v. 736, p. 75–84, https://doi.org/10.1016/j.tecto.2018.04.020.

Haile, B.G., Line, L.H., Klausen, T.G., Olaussen, S., Eide, C.H., Jahren, J., and Hellevang, H., 2021, Quartz overgrowth textures and fluid inclusion thermometry evidence for basin-scale sedimentary recycling: An example from the Mesozoic Barents Sea Basin: Basin Research, v. 33, p. 1697–1710, https://doi.org/10.1111/bre.12531.

Harstad, T.S., Mørk, E.M.B., and Slagstad, T., 2020, The importance of trace element analyses in detrital Cr-spinel provenance studies: An example from the Upper Triassic of the Barents Shelf: Basin Research, https://doi.org/10.1111/bre.12502.

Helland-Hansen, W., Sømme, T.O., Martinsen, O.J., et al., 2016, Deciphering Earth's natural hourglasses: Perspectives on source-to-sink analysis: Journal of Sedimentary Research, v. 86, no. 9, p. 1008–1033, https://doi.org/10.2110/jsr.2016.56.

Khudoley, A.K., et al., 2018, Late Paleozoic–Mesozoic tectonic evolution of the Eastern Taimyr-Severnaya Zemlya Fold and Thrust Belt and adjoining Yenisey-Khatanga depression: Journal of Geodynamics, v. 119, p. 221–241, https://doi.org/10.1016/j.jog.2018.02.002.

Khudoley, A.K., et al., 2019, A reconnaissance provenance study of Triassic–Jurassic clastic rocks of the Russian Barents Sea: GFF, v. 141, no. 4, p. 263–271, https://doi.org/10.1080/11035897.2019.1621372.

Klausen, T.G., Ryseth, A.E., Helland-Hansen, W., Gawthorpe, R., and Laursen, I., 2014, Spatial and temporal changes in geometries of fluvial channel bodies from the Triassic Snadd Formation of offshore Norway: Journal of Sedimentary Research, v. 84, no. 7, p. 567–585, https://doi.org/10.2110/jsr.2014.47.

Klausen, T.G., Ryseth, A.E., Helland-Hansen, W., Gawthorpe, R., and Laursen, I., 2015, Regional development and sequence stratigraphy of the Middle to Late Triassic Snadd formation, Norwegian Barents Sea: Marine and Petroleum Geology, v. 62, p. 102–122, https://doi.org/10.1016/j.marpetgeo.2015.02.004.

Klausen, T.G., Ryseth, A., Helland-Hansen, W., and Gjelberg, H.K., 2016, Progradational and backstepping shoreface deposits in the Ladinian to Early Norian Snadd Formation of the Barents Sea: Sedimentology, v. 63, p. 893–916, https://doi.org/10.1111/sed.12242.

Klausen, T.G., Müller, R., Slama, J., and Helland-Hansen, W., 2017, Evidence for Late Triassic provenance areas and Early Jurassic sediment supply turnover in the Barents Sea Basin of northern Pangea: Lithosphere, v. 9, no. 1, p. 14–28, https://doi.org/10.1130/L556.1.

Klausen, T.G., Torland, J.A., Eide, C.H., Alaei, B., Olaussen, S., and Chiarellaet, D., 2018, Clinoform development and topset evolution in a mud-rich delta—the Middle Triassic Kobbe Formation, Norwegian Barents Sea: Sedimentology, v. 65, no. 4, p. 1132–1169, https://doi.org/10.1111/sed.12417.

Klausen, T.G., Müller, R., Poyatos-Moré, M., Olaussen, S., and Stueland, E., 2019, Tectonic, provenance and sedimentological controls on reservoir characteristics in the Upper Triassic–Middle Jurassic Realgrunnen Subgroup, SW Barents Sea, in Hendry, J., Burgess, P., Hunt, D., Janson, X., and Zampetti, V., eds., Seismic Characterization of Carbonate Platforms and Reservoirs: Geological Society, London, Special Publication 495, https://doi.org/10.1144/SP495-2018-165.

Klausen, T.G., Nyberg, B., and Helland-Hansen, W., 2019, The largest delta plain in Earth's history: Geology, v. 47, no. 5, p. 470–474, https://doi.org/10.1130/G45507.1.

Kurapov, M., Ershova, V., Khudoley, A., Luchitskaya, M., Makariev, A., Makarieva, E., and Vishnevskaya, I., 2020, Late Palaeozoic magmatism of Northern Taimyr: new insights into the tectonic evolution of the Russian High Arctic: International Geology Review, https://doi.org/10.1080/00206814.2020.1818300.

Leech, M.L., and Stockli, D.F., 2000, The late exhumation history of the ultrahigh-pressure Maksyutov Complex, south Ural Mountains, from new apatite fission track data: Tectonics, v. 19, no. 1, p. 153–167, https://doi.org/10.1029/1999TC900053.

Li, S., Wang, T., Wilde, S.A., and Tong, Y., 2013, Evolution, source and tectonic significance of Early Mesozoic granitoid magmatism in the Central Asian Orogenic Belt (central segment): Earth-Science Reviews, v. 126, p. 206–234, https://doi.org/10.1016/j.earscirev.2013.06.001.

Lloyd, M.J., Nichols, G.J., and Friend, P.F., 1998, Oligo-Miocene alluvial-fan evolution at the southern Pyrenean thrust front, Spain: Journal of Sedimentary Research, v. 68, no. 5, p. 869–878, https://doi.org/10.2110/jsr.68.869.

Mark, N., Schofield, N., Gardiner, D., Holt, L., Grove, C., Watson, D., Alexander, A., and Poore, H., 2019, Overthickening of sedimentary sequences by igneous intrusions: Journal of the Geological Society, v. 176, no. 1, p. 46–60, https://doi.org/10.1144/jgs2018-112.

Meshcheryakov, K.A., and Karaseva, T.V., 2010, The formation peculiarities of the Triassic troughs of the north of Western Siberia [in Russian]: Petroleum Geology—Theoretical and Applied Studies, v. 5, p. 9–9.

Meshcheryakov, K.A., Karaseva, T.V., Kozhanov, D.D., et al., 2019, The Triassic oil and gas complex is a potential object for the growth of the resource base of Western Siberia: Bulletin of Perm University: Geology, v. 18, no. 1.

Miller, E.L., et al., 2006, New insights into Arctic paleogeography and tectonics from U-Pb detrital zircon geochronology: Tectonics, v. 25, no. 3, https://doi.org/10.1029/2005TC001830.

Miller, E.L., Soloviev, A.V., Prokopiev, A.V., Toro, J., Harris, D., Kuzmichev, A.B., and Gehrels, G.E., 2013, Triassic river systems and the paleo-Pacific margin of northwestern Pangea: Gondwana Research, v. 23, no. 4, p. 1631–1645, https://doi.org/10.1016/j.gr.2012.08.015.

Miller, E.L., et al., 2018, Circum-Arctic Lithosphere Evolution (CALE) Transect C: displacement of the Arctic Alaska–Chukotka microplate towards the Pacific during opening of the Amerasia Basin of the Arctic, *in* Pease, V., and Coakley, B., eds., Circum-Arctic Lithosphere Evolution: Geological Society, London, Special Publication 460, no. 1, p. 57, https://doi.org/10.1144/SP460.9.

Milliman, J.D., and Farnsworth, K.L., 2013, River discharge to the coastal ocean: A global synthesis: Cambridge, UK, Cambridge University Press, 394 p., https://doi.org/10.1017/CBO9780511781247.

Molnar, P., and Lyon-Caen, H., 1988, Some simple physical aspects of the support, structure, and evolution of mountain belts. Processes in continental lithospheric deformation, *in* Clark, S.P., Jr., Burchfiel, B.C., and Suppe, J., eds., Processes in Continental Lithospheric Deformation: Geological Society of America Special Paper 218, p. 179–207, http://doi.org/10.1130/SPE218-p179.

Morakhovskaja, E.D., 2000, Triassic deposits of Timan-Ural region (key sections, stratigraphy, correlation) [in Russian]: Biochronology and correlation of Phanerozoic of oil and gas basins of Russia: St. Petersburg, VNI-GRI, v. 1, 80 p.

Mørk, M.B.E., 1999, Compositional variations and provenance of Triassic sandstones from the Barents Shelf: Journal of Sedimentary Research, v. 69, no. 3, p. 690–710, https://doi.org/10.2110/jsr.69.690.

Mueller, S., Hounslow, M.W., and Kürschner, W.M., 2016, Integrated stratigraphy and palaeoclimate history of the Carnian Pluvial Event in the Boreal realm; new data from the Upper Triassic Kapp Toscana Group in central Spitsbergen (Norway): Journal of the Geological Society, v. 173, no. 1, p. 186–202, https://doi.org/10.1144/jgs2015-028.

Müller, R., Klausen, T.G., Faleide, J.I., Olaussen, S., Eide, C.H., and Suslovad, A., 2019, Linking regional unconformities in the Barents Sea to compression-induced forebulge uplift at the Triassic-Jurassic transition: Tectonophysics, v. 765, p. 35–51, https://doi.org/10.1016/j.tecto.2019.04.006.

Nikishin, A., et al., 1996, Late Precambrian to Triassic history of the East European Craton: Dynamics of sedimentary basin evolution: Tectonophysics, v. 268, no. 1–4, p. 23–63, https://doi.org/10.1016/S0040-1951(96)00228-4.

Nikishin, A., Ziegler, P., Abbott, D., Brunet, M.-F., and Cloetingh, S., 2002, Permo–Triassic intraplate magmatism and rifting in Eurasia: Implications for mantle plumes and mantle dynamics: Tectonophysics, v. 351, no. 1–2, p. 3–39, https://doi.org/10.1016/S0040-1951(02)00123-3.

Nikishin, A., Sobornov, K., Prokopiev, A., and Frolov, S.V., 2010, Tectonic evolution of the Siberian platform during the Vendian and Phanerozoic: Moscow University Geology Bulletin, v. 65, no. 1, p. 1–16, https://doi.org/10.3103/S0145875210010011.

Nikishin, A.M., et al., 2019, Geological structure and history of the Arctic Ocean based on new geophysical data: Implications for paleoenvironment and paleoclimate. Part 2. Mesozoic to Cenozoic geological evolution: Earth-Science Reviews, v. 217, no. 103034, https://doi.org/10.1016/j.earscirev.2019.103034.

Norina, D.A., Stoupakova, A.V., and Kiryukhina, T.A., 2014, Depositional environments and the hydrocarbon generative potential of Triassic source rocks of the Barents Sea basin: Moscow University Geology Bulletin, v. 69, no. 1, p. 1–10, https://doi.org/10.3103/S0145875214010062.

Nyberg, B., Helland-Hansen, W., Gawthorpe, R., Tillmans, F., and Sandbakken, P., 2021, Assessing first-order BQART estimates for ancient source-to-sink mass budget calculations: Basin Research, v. 33, p. 2435–2452, https://doi.org/10.1111/bre.12563.

Nystuen, J.P., Kjemperud, A.V., Müller, R., Adestål, V. and Schomacker, E.R., 2014, Late Triassic to Early Jurassic climatic change, northern North Sea region, *in* Stevens, T., Martinius, A.W., Ravnås, R., Howell, J.A., Steel, R.J., and Wonham, J.P., eds., Impact on alluvial architecture, palaeosols and clay mineralogy: Depositional Systems to Sedimentary Successions on the Norwegian Continental Margin, https://doi.org/10.1002/9781118920435.ch3.

Ogg, J.G., Huang, C., and Hinnov, L., 2014, Triassic timescale status: A brief overview: Albertiana, v. 41, p. 3–30.

Omma, J.E., 2009, Provenance of late Paleozoic and Mesozoic sediment to key Arctic basins [Ph.D. dissertation]: Implications for the opening of the Arctic Ocean: Cambridge, UK, University of Cambridge, 222 p.

Omma, J., Pease, V., and Scott, R., 2011, U–Pb SIMS zircon geochronology of Triassic and Jurassic sandstones on northwestern Axel Heiberg Island, northern Sverdrup Basin, Arctic Canada, *in* Spencer, A.M., Embry, A.F., Gautier, D.L., Stoupakova, A.V., and Sørensen, K., eds., Arctic Petroleum Geology: Geological Society, London, Memoir 35, p. 559–566, https://doi.org/10.1144/M35.37.

Parrish, J.T., 1998, Interpreting Pre-Quaternary Climate from the Geologic Record: New York, Columbia University Press, 354 p.

Paterson, N.W., and Mangerud, G., 2019, A revised palynozonation for the Middle–Upper Triassic (Anisian–Rhaetian) Series of the Norwegian Arctic: Geological Magazine, v. 157, p. 1568–1592, https://doi.org/10.1017/S0016756819000906.

Peace, A.L., Phethean, J., Franke, D., Foulger, G.R., Schiffer, C., Welford, J.K., McHone, G., Rocchi, S., Schnabel, M., and Doré, A.G., 2020, A review of Pangaea dispersal and Large Igneous Provinces—In search of a causative mechanism: Earth-Science Reviews, v. 206, no. 102902, https://doi.org/10.1016/j.earscirev.2019.102902.

Pease, V., 2011, Chapter 20: Eurasian orogens and Arctic tectonics: an overview, *in* Spencer, A.M., Embry, A.F., Gautier, D.L., Stoupakova, A.V., and Sørensen, K., eds., Arctic Petroleum Geology: Geological Society, London, Memoir 35, p. 311–324, https://doi.org/10.1144/M35.20.

Péron, S., Bourquin, S., Fluteau, F., and Guillocheau, F., 2005, Paleoenvironment reconstructions and climate simulations of the Early Triassic: Impact of the water and sediment supply on the preservation of fluvial systems: Geodinamica Acta, v. 18, no. 6, p. 431–446, https://doi.org/10.3166/ga.18.431-446.

Petrov, O.V., et al., 2012, Geological map of Russia and adjoining water areas [in Russian]: Poyasnitelnaya zapiska / Ministry of Natural Resources and Environment of the Russian Federation, Federal Agency for Subsoil Management, Russian Geological Research Institute, A.P. Karpinsky (VSEGEI), scale 1:2,500,000, 58 p.

Petrov, O.V., et al., 2016, Russian scientific school of geological cartography in compiling new generation of the state geological maps of the Russian Federation, its continental shelf and abyssal oceanic margins of Eurasia and Circumpolar Arctic [in Russian]: Regional Geology and Metallogeny, v. 67, no. 67, p. 6–18.

Polteau, S., Hendriks, B.W.H., Planke, S., Ganerød, M., Fernando, C., Corfu, F., Inge, J., Faleid, J.I., Midtkandal, I., Svensen, H.S., and Myklebust, R., 2016, The Early Cretaceous Barents Sea Sill Complex: Distribution, ^{40}Ar/^{39}Ar geochronology, and implications for carbon gas formation: Palaeogeography, Palaeoclimatology, Palaeoecology, v. 441, p. 83–95, https://doi.org/10.1016/j.palaeo.2015.07.007.

Prischepa, O., Bazhenova, T., and Bogatskii, V., 2011, Petroleum systems of the Timan–Pechora sedimentary basin (including the offshore Pechora Sea): Russian Geology and Geophysics, v. 52, no. 8, p. 888–905, https://doi.org/10.1016/j.rgg.2011.07.011.

Puchkov, V.N., 2009, The evolution of the Uralian orogen, *in* Murphy, J.B., Keppie, J.D., and Hynes, A.J., Ancient Orogens and Modern Analogues: Geological Society, London, Special Publication 327, no. 1, p. 161–195, https://doi.org/10.1144/SP327.9.

Reichow, M.K., et al., 2009, The timing and extent of the eruption of the Siberian Traps large igneous province: Implications for the end-Permian environmental crisis: Earth and Planetary Science Letters, v. 277, no. 1, p. 9–20, https://doi.org/10.1016/j.epsl.2008.09.030.

Rossi, V.M., Paterson, N.W., Helland-Hansen, W., Klausen, T.G., and Haug Eide, C., 2019, Mud-rich delta-scale compound clinoforms in the Triassic shelf of northern Pangea (Havert Formation, south-western Barents Sea): Sedimentology, v. 66, no. 6, https://doi.org/10.1111/sed.12598.

Ruffell, A., Simms, M., and Wignall, P., 2016, The Carnian Humid Episode of the late Triassic: A review: Geo-

logical Magazine, v. 153, no. 2, p. 271–284, https://doi.org/10.1017/S0016756815000424.

Saraev, S., Baturina, T., and Travin, A., 2011, Petrology, sedimentology, geochemistry, and absolute age of Triassic volcanosedimentary rocks from the southwest of the West Siberian geosyneclise (Kurgan Region): Russian Geology and Geophysics, v. 52, no. 8, p. 871–887, https://doi.org/10.1016/j.rgg.2011.07.010.

Scotese, C., and Moore, T., 2014, Atlas of Phanerozoic Temperatures (Mollweide Projection), Volumes 1–6: Evanston, Illinois, USA, PALEOMAP Project Paleo-Atlas for ArcGIS, PALEOMAP Project, https://doi.org/10.13140/2.1.4904.6086.

Scotese, C.R., and Wright, N., 2018, PALEOMAP paleodigital elevation models (PaleoDEMS) for the Phanerozoic: https://www. earthbyte. org/paleodem-resource-scotese-and-wright-2018.

Sellwood, B.W., and Valdes, P.J., 2006, Mesozoic climates: General circulation models and the rock record: Sedimentary Geology, v. 190, no. 1–4, p. 269–287, https://doi.org/10.1016/j.sedgeo.2006.05.013.

Şengör, A., and Natal'in, B., 2004, Phanerozoic analogues of Archaean oceanic basement fragments: Altaid ophiolites and ophirags: Developments in Precambrian Geology, v. 13, p. 675–726, https://doi.org/10.1016/S0166-2635(04)13021-1.

Şengör, A.C., and Natal'In, B.A., 1996, Turkic-type orogeny and its role in the making of the continental crust: Annual Review of Earth and Planetary Sciences, v. 24, no. 1, p. 263–337, https://doi.org/10.1146/annurev.earth.24.1.263.

Shephard, G., Müller, D., and Seton, M., 2013, The tectonic evolution of the Arctic since Pangea breakup: Integrating constraints from surface geology and geophysics with mantle structure: Earth-Science Reviews, v. 124, p. 148–183, https://doi.org/10.1016/j.earscirev.2013.05.012.

Simms, M.J., and Ruffell, A.H., 1989, Synchroneity of climatic change and extinctions in the Late Triassic: Geology, v. 17, no. 3, p. 265–268, https://doi.org/10.1130/0091-7613(1989)017<0265:SOCCAE>2.3.CO;2.

Soloviev, A.V., Zaionchek, A.V., Suprunenko, O.I., et al., 2015, Evolution of the provenances of Triassic rocks in Franz Josef Land: U/Pb LA-ICP-MS dating of the detrital zircon from Well Severnaya: Lithology and Mineral Resources, v. 50, p. 102–116, https://doi.org/10.1134/S0024490215020054.

Sømme, T., Dore, A., Lundin, E., and Tørudbakken, B.O., 2018, Triassic–Paleogene paleogeography of the Arctic: Implications for sediment routing and basin fill: AAPG Bulletin, v. 102, p. 2481–2517, https://doi.org/10.1306/05111817254.

Sømme, T.O., Helland-Hansen, W., Martinsen, O.J., and Thurmond, J.B., 2009, Relationships between morphological and sedimentological parameters in source-to-sink systems: A basis for predicting semi-quantitative characteristics in subsurface systems: Basin Research, v. 21, no. 4, p. 361–387, https://doi.org/10.1111/j.1365-2117.2009.00397.x.

Sun, Y., et al., 2012, Lethally hot temperatures during the Early Triassic greenhouse: Science, v. 338, no. 6105, p. 366–370, https://doi.org/10.1126/science.1224126.

Surkov, V.S., and Zhero, O.G., 1981, The basement and development of the platform cover of the West Siberian plate: M. Nedra (In Russian).

Syvitski, J.P., and Milliman, J.D., 2007, Geology, geography, and humans battle for dominance over the delivery of fluvial sediment to the coastal ocean: The Journal of Geology, v. 115, no. 1, p. 1–19, https://doi.org/10.1086/509246.

Tevelev, A.V., 2013, Types of posttrap hypabyssal granitoids of the Circum-Siberian belt (Tipy posletrappovykh gipabissal'nykh granitoidov Tsirkum-Sibirskogo poyasa, In Russian): Moscow University Bulletin, Series 4: Geology, v. 4.

Trotter, J.A., Williams, I.S., Nicora, A., Mazza, M., and Rigo, M., 2015, Long-term cycles of Triassic climate change: A new δ^{18}O record from conodont apatite: Earth and Planetary Science Letters, v. 415, p. 165–174, https://doi.org/10.1016/j.epsl.2015.01.038.

Vernikovsky, V.A., Pease, V.L., Vernikovskaya, A.E., Romanov, A.P., Gee, D.G., and Travin, A.V., 2003, First

report of early Triassic A-type granite and syenite intrusions from Taimyr: Product of the northern Eurasian superplume?: Lithos, v. 66, no. 1–2, p. 23–36, https://doi.org/10.1016/S0024-4937(02)00192-5.

Vernikovsky, V.A., Vernikovskaya, A., Proskurnin, V., Matushkin, N., Proskurnina, M., Kadilnikov, P., Larionov, A., and Travin, A., 2020, Late Paleozoic–Early Mesozoic granite magmatism on the Arctic margin of the Siberian craton during the Kara-Siberia oblique collision and plume events: Minerals, v. 10, no. 6, p. 571, https://doi.org/10.3390/min10060571.

Vigran, J. O., Mangerud, G., Mørk, A., Worsley, D., and Hochuli, P.A., 2014, Palynology and Geology of the Triassic Succession of Svalbard and the Barents Sea (Volume 14): Trondheim, Norway, Norges geologiske undersokelse Special Publication, 269 p.

Vyssotski, A., Vyssotski, V., and Nezhdanov, A., 2006, Evolution of the West Siberian basin: Marine and Petroleum Geology, v. 23, no. 1, p. 93–126, https://doi.org/10.1016/j.marpetgeo.2005.03.002.

Wang, T., et al., 2017, Phanerozoic granitoids in the central and eastern parts of Central Asia and their tectonic significance: Journal of Asian Earth Sciences, v. 145, p. 368–392, https://doi.org/10.1016/j.jseaes.2017.06.029.

Wilhem, C., Windley, B.F., and Stampfli, G.M., 2012, The Altaids of Central Asia: A tectonic and evolutionary innovative review: Earth-Science Reviews, v. 113, no. 3–4, p. 303–341, https://doi.org/10.1016/j.earscirev.2012.04.001.

Winguth, A.M., Shields, C.A., and Winguth, C., 2015, Transition into a Hothouse World at the Permian–Triassic boundary—A model study: Palaeogeography, Palaeoclimatology, Palaeoecology, v. 440, p. 316–327, https://doi.org/10.1016/j.palaeo.2015.09.008.

Worsley, D., 2008, The post-Caledonian development of Svalbard and the western Barents Sea: Polar Research, v. 27, no. 3, p. 298–317, https://doi.org/10.1111/j.1751-8369.2008.00085.x.

Xiao, W., Windley, B.F., Sun, S., Li, J., Huang, B., Han, C., Yuan, C., Sun, M., and Chen, H., 2015, A tale of amalgamation of three Permo-Triassic collage systems in Central Asia: Oroclines, sutures, and terminal accretion: Annual Review of Earth and Planetary Sciences, v. 43, p. 477–507, https://doi.org/10.1146/annurev-earth-060614-105254.

Zhang, J., Covault, J., Pyrcz, M., Sharman, G., Carvajal, C., and Milliken, K., 2018a, Quantifying sediment supply to continental margins: Application to the Paleogene Wilcox Group, Gulf of Mexico: American Association of Petroleum Geologists Bulletin, v. 102, no. 9, p. 1685–1702, https://doi.org/10.1306/01081817308.

Zhang, S.-H., Zhao, Y., Kröner, A., Liu, X.-M., Xie, L.-W., and Chen, F.K., 2009, Early Permian plutons from the northern North China Block: Constraints on continental arc evolution and convergent margin magmatism related to the Central Asian Orogenic Belt: International Journal of Earth Sciences, v. 98, no. 6, p. 1441–1467, https://doi.org/10.1007/s00531-008-0368-2.

Zhang, X., Pease, V., Carter, A., Kostuychenko, S., Suleymanov, A., and Scott, R., 2018b, Timing of exhumation and deformation across the Taimyr fold–thrust belt: Insights from apatite fission track dating and balanced cross-sections *in* Pease, V., and Coakley, B., eds., Circum-Arctic Lithosphere Evolution: Geological Society, London, Special Publication 460, no. 1, p. 315–333, https://doi.org/10.1144/SP460.3.

Zuchuat, V., 2014. A Sedimentary Investigation of the Lower Triassic Formations and Their Underlying Permo-Carboniferous Units Across Spitsbergen [M.S. thesis]: Svalbard, Norway, Norwegian University of Science and Technology, 153 p.

Geological Society of America Bulletin